

# Increasing-Margin Adversarial (IMA) Training to Improve Adversarial Robustness of Neural Networks

*Linhai Ma & Liang Liang*  
*l.ma@miami.edu & liang.liang@miami.edu*

## Abstract

Convolutional neural networks (CNN) have surpassed traditional methods for medical image classification. However, CNNs are vulnerable to adversarial attacks which may lead to disastrous consequences in medical applications. Although adversarial noises are usually generated by attack algorithms, white-noise-induced adversarial samples can exist, and therefore the threats are real. In this study, we propose a novel training method, named IMA, to improve CNN robustness against adversarial noises. During training, the IMA method increases the margins of training samples in the input space, i.e., moving CNN decision boundaries far away from the training samples to improve robustness. The IMA method is evaluated on publicly available datasets under strong 100-PGD white-box adversarial attacks, and the results show that the proposed method significantly improved image classification and segmentation accuracy on noisy data while keeping a high accuracy on clean data. We hope our approach may facilitate the development of robust applications in the medical field. The implementation will be released publically after this paper is published. If interested, please contact the authors.

## 1 Introduction

Deep neural networks (DNNs), especially convolutional neural networks (CNNs), have become the first choice for automated image analysis due to their superior performance. However, recent studies have shown that DNNs are not robust to adversarial noises. Adversarial noise was first discovered by [Szegedy et al.(2013)Szegedy, Zaremba, Sutskever, Bruna, Erhan, Goodfellow, and Fergus] and then explained by [Goodfellow et al.(2015)Goodfellow, Shlens, and Szegedy]. Adversarial noises can significantly affect robustness of DNNs for a wide range of image classification applications [Akhtar & Mian(2018)Akhtar and Mian, Graese et al.(2016)Graese, Rozsa, and Boulton, Mirjalili & Ross(2017)Mirjalili and Ross, Eykholt et al.(2018)Eykholt, Evtimov, Fernandes, Li, Rahmati, Xiao, Prakash, Kohno, and Song]. DNN-based image segmentation can also be affected by adversarial noises because image segmentation is often realized by pixel classification.

The COVID-19 pandemic has caused the death of more than 1 million people [WHO(2020)]. A large-scale study in China shows that CT had higher sensitivity for the diagnosis of COVID-19 as compared with initial reverse-transcription polymerase chain reaction (RT-PCR) from swab samples [Ai et al.(2020)Ai, Yang, Hou, Zhan, Chen, Lv, Tao, Sun, and Xia]. As reviewed in [Shi et al.(2020)Shi,

Wang, Shi, Wu, Wang, Tang, He, Shi, and Shen], many DNN models for COVID-19 diagnosis from CT images have been developed and achieved very high classification accuracy. However, none of these studies [Shi et al.(2020)Shi, Wang, Shi, Wu, Wang, Tang, He, Shi, and Shen] considered DNN robustness against adversarial noises. We modified a Resnet-18 model [He et al.(2016)He, Zhang, Ren, and Sun] and trained it on a public COVID-19 CT image dataset [Soares et al.(2020)Soares, Angelov, Biaso, Froes, and Abe], and then the model robustness is tested (details in section 3.4). Fig. 1 shows a CT image (denoted by  $x$ ) of a lung that was infected by COVID-19 and correctly classified as infected. After adding a small amount of noise  $\delta$  to the image  $x$ , the noisy image  $x + \delta$  is classified as uninfected. On the test set, although the model achieved  $\geq 95\%$  accuracy on original clean images, its accuracy dropped to zero on small noise levels. This non-robust model clearly cannot be used in real clinical applications. Researchers have been working on DNN adversarial robustness from different aspects[Ruoss et al.(2021)Ruoss, Baader, Balunovic, and Vechev, Sarkar et al.(2021)Sarkar, Sarkar, and Balasubramanian, Yang et al.(2021)Yang, Guo, Wang, and Xu, Bui et al.(2021)Bui, Le, Zhao, Montague, de Vel, Abraham, and Phung, Fan & Li(2021)Fan and Li, Gokhale et al.(2021)Gokhale, Anirudh, Kailkhura, Thiagarajan, Baral, and Yang, Jia et al.(2021a)Jia, Cao, and Gong, Li et al.(2021)Li, Li, Pan, and Zhu, Liang & Huang(2021)Liang and Huang, Ning et al.(2021)Ning, Tao, Chen, and Huang, Agarwal et al.(2021)Agarwal, Vatsa, and Singh, Wang & He(2021)Wang and He, Deng et al.(2021)Deng, Yang, Xu, Su, and Zhu, Rampini et al.(2021)Rampini, Pestarini, Cosmo, Melzi, and Rodola, Wu et al.(2021a)Wu, Liu, Huang, Wang, and Lin, Awasthi et al.(2021)Awasthi, Yu, Ferng, Tomkins, and Juan, Cazenavette et al.(2021)Cazenavette, Murdock, and Lucey, Jia et al.(2021b)Jia, Song, Ma, and Yang, Chen et al.(2021)Chen, Kung, and Chen, Wu et al.(2021b)Wu, Su, Lyu, and King, Yu et al.(2021)Yu, Gao, and Xu, Elliott et al.(2021)Elliott, Law, and Russell, Gong et al.(2021)Gong, Ren, Ye, and Liu, Wang et al.(2021)Wang, He, Peng, Shao, Yang, Zhou, and Hogg].

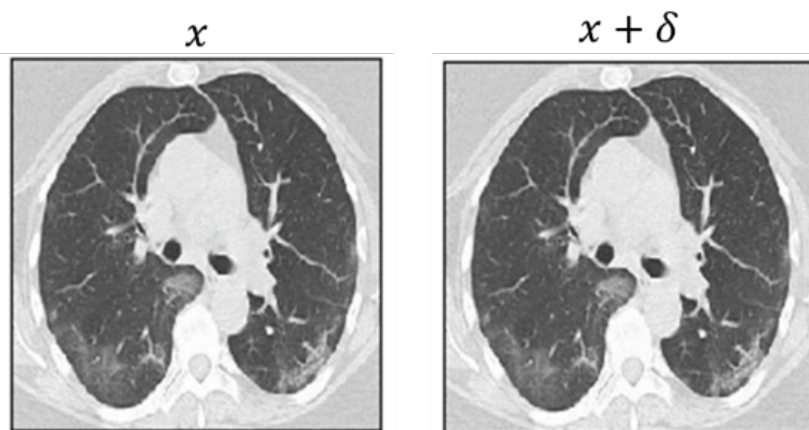


Figure 1: An example of clean and noisy images.

There are mainly two categories of adversarial attacks: white-box attack [Goodfellow et al.(2015)Goodfellow, Shlens, and Szegedy, Kurakin et al.(2016)Kurakin, Goodfellow, Bengio, et al., Carlini & Wagner(2017)Carlini and Wagner, Madry et al.(2018)Madry, Makelov, Schmidt, Tsipras, and Vladu] and black-box attack [Chen et al.(2017)Chen, Zhang, Sharma, Yi, and Hsieh, Ilyas et al.(2018)Ilyas, Engstrom, Athalye, and Lin]. Researchers have explored many ideas to improve robustness, but many of those have been shown to be ineffective [Uesato et al.(2018)Uesato, O’donoghue, Kohli, and Oord, Tramer et al.(2020)Tramer, Carlini, Brendel, and Madry]. A general and effective strategy is adversarial training [Goodfellow et al.(2015)Goodfellow, Shlens, and Szegedy, Madry et al.(2018)Madry, Makelov, Schmidt, Tsipras, and Vladu, Miyato et al.(2018)Miyato, Maeda, Koyama, and Ishii, Ding et al.(2020)Ding, Sharma, Lui, and Huang, Athalye et al.(2018)Athalye, Carlini, and Wagner, Cheng et al.(2020)Cheng, Lei, Chen, Dhillon, and Hsieh, Wang et al.(2020)Wang, Zou, Yi, Bailey, Ma, and Gu], and the basic idea is to use adversarial attack algorithms to generate noisy samples and add those samples to the training set. Through adversarial training, a DNN model can learn from the noisy samples and become robust to noises. Vanilla adversarial training [Goodfellow et al.(2015)Goodfellow, Shlens, and Szegedy, Kurakin et al.(2016)Kurakin, Goodfellow, Bengio, et al.] is straightforward but problematic. It wrongly assumes that the perturbation is a fixed constant for all training samples. However, every sample may have different intrinsic robustness [Cheng et al.(2020)Cheng, Lei, Chen, Dhillon, and Hsieh]. Generative adversarial training has been directly applied to improve robustness; however, it can only defend against black-box attack [Wang & Yu(2019)Wang and Yu].

In this paper, we propose a novel adversarial training method, Increasing-Margin Adversarial (IMA) Training, to improve DNN robustness (our contribution-1). Our method aims to increase margins of training samples by moving decision boundaries far away from the samples gradually to improve robustness. We evaluated our method on datasets with 100-PGD white-box attack and compared it with the other six adversarial defense methods for image classification tasks. The results show that our proposed method can improve DNN robustness while keeping a satisfactory accuracy on clean data, better than MMA [Ding et al.(2020)Ding, Sharma, Lui, and Huang] (a state-of-the-art method). The experiment also demonstrates that our IMA method can be used not only for image classification tasks but also for image segmentation tasks (our contribution-2).

## 2 Methodology

### 2.1 Adversarial Attack and Neural Network Robustness

To evaluate the robustness of different adversarial training methods, we used projected gradient descent (PGD) [Madry et al.(2018)Madry, Makelov, Schmidt, Tsipras, and Vladu, Kurakin et al.(2016)Kurakin, Goodfellow, Bengio, et al.] to generate adversarial noises, which is widely used for method evaluation [Uesato

et al.(2018)Uesato, O’donoghue, Kohli, and Oord, Tramer et al.(2020)Tramer, Carlini, Brendel, and Madry]. For the convenience of the reader, we briefly describe PGD: Let  $x$  denote an input sample and  $y$  be the true class label. Let  $J(x)$  denote the scalar objective function of PGD, which could be the cross-entropy loss function or other classification loss functions. Let  $\delta$  denote the adversarial noise, and its magnitude is  $\varepsilon$  which is measured by the vector Lp norm of  $\delta$ , i.e.,  $\varepsilon = \|\delta\|_p$ , where  $p$  is inf or 2 usually. PGD adds noises to  $x$  iteratively:

$$x_{(i)} = \text{clip}(x_{(i-1)} + \eta \cdot h(J'(x_{(i-1)}))) \tag{1}$$

where  $\eta$  is step size,  $J'(x) = \frac{\partial J}{\partial x}$ , and  $i$  is iteration index.  $x_{(0)} = x + \xi$ , where  $\xi$  is random noise with  $\|\xi\|_p \leq \varepsilon$ . The clip operation in Eq.(1) ensures that  $\|x_{(i)} - x\|_p \leq \varepsilon$  (called  $\varepsilon$ -ball). If  $x$  is an image, the clip operation also ensures that pixel values stay within the feasible range (e.g. 0 to 1). If L-inf norm is used,  $h(J')$  is the sign function; and if L2 norm is used, then  $h(J')$  normalizes  $J'$  by its L2 norm. The total adversarial noise is  $\delta = x_{(N_{PGD})} - x$ , and  $N_{PGD}$  is the number of iterations.  $\eta$  is usually set to  $\alpha \cdot \varepsilon / N_{PGD}$ , and therefore the algorithm may sweep the  $\varepsilon$ -ball  $\alpha$  times ( $\alpha \geq 1$ ) within  $N_{PGD}$  iterations. By adding the adversarial noise  $\delta$  to the input  $x$ , the objective function  $J(x + \delta)$  will be significantly larger than  $J(x)$ , leading to wrong classification of the noisy sample  $x + \delta$ .

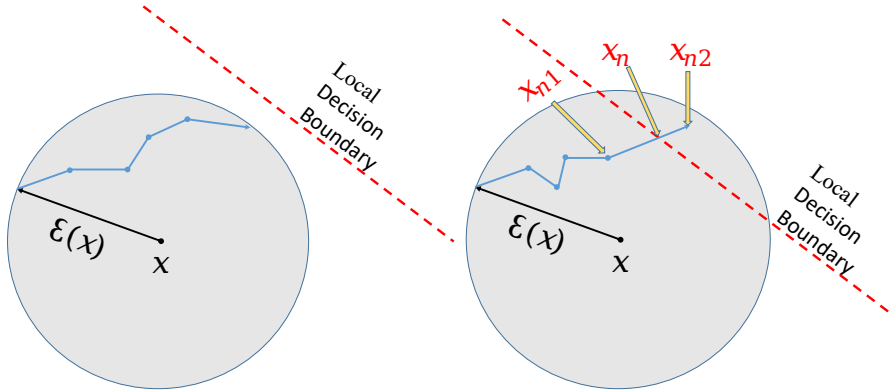


Figure 2: Left: case-0 in Algorithm 3; Right: case-1 in Algorithm 3.

It is easy to understand the robustness issue through Eq.(1) and Fig. 2. Given a trained classifier, if a sample  $x$  is very close to the decision boundary of the classifier, then one could add a small noise  $\delta$  to  $x$  such that  $x + \delta$  goes across the decision boundary and is wrongly classified. As shown in section 3, using standard training with cross-entropy loss and clean data, the decision boundaries of the trained classifier will often be very close to the samples; as a result, the accuracy can drop to zero upon very small noises.

To improve robustness, vanilla adversarial training [Goodfellow et al.(2015)Goodfellow,

Shlens, and Szegedy, Kurakin et al.(2016)Kurakin, Goodfellow, Bengio, et al.] based on PGD can be used: given the maximum noise level  $\varepsilon = \varepsilon_{max}$ , generate a noisy sample  $x_\varepsilon = PGD(x, y, \varepsilon)$  for every clean sample  $x$  in training set; use the clean samples and noisy samples together to train the model. The loss function is given in [Goodfellow et al.(2015)Goodfellow, Shlens, and Szegedy]:

$$L_{adv} = (L_{ce}(x, y) + L_{ce}(x_\varepsilon, y))/2 \tag{2}$$

In practice, the loss is accumulated over each mini-batch.  $L_{ce}$  is the cross-entropy loss. As shown in the experiments, the vanilla adversarial training is very sensitive to the user-defined noise level  $\varepsilon_{max}$ .

## 2.2 Increasing-Margin Adversarial (IMA) Training

We developed a novel method, Increasing-Margin Adversarial (IMA) training, to enhance DNN classifier robustness. As its name indicates, IMA is a type of adversarial training: it generates noisy samples and trains a DNN model on clean and noisy samples. IMA algorithms are significantly different from the other adversarial training algorithms.

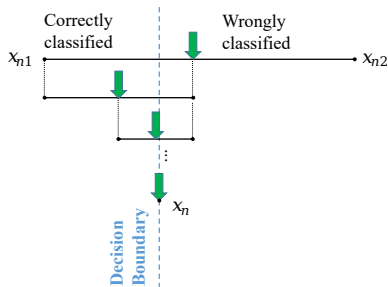


Figure 3: Binary search in BPGD (Algorithm 3).

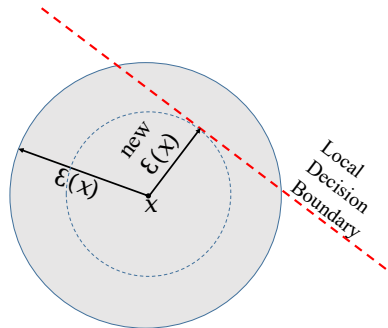


Figure 4: Shrink Margin in Algorithm 2.

IMA training includes two alternating sub-processes: Algorithm 1 to compute loss and update the DNN model, and Algorithm 2 to update margin estimation. In Algorithm 1, by minimizing the loss on clean and noisy data, the model will reach a balance between robustness and accuracy on clean data. In Algorithm 2, the sample margins are updated after each epoch. These estimated margins are used for generating noisy samples for training the model in the next epoch.

Our IMA method tries to generate adversarial samples on decision boundaries as much as possible: adding too much noise to a training sample may lead to low accuracy on clean samples, but adding too little noise may have no effect on robustness. Since the distance between a training sample and a decision boundary is different for different training samples, the noises added to the

---

**Algorithm 1** compute loss and update model in an epoch

---

**Input:**  $S = (x, y)$  is the training set, containing pairs of clean sample  $x$  and true label  $y$ .  $f$  is the DNN model and  $\hat{y} = f(x)$ .  $\mathcal{E}$  is an array containing the estimated margins of individual training samples.  $\beta$  is a scalar coefficient. In a batch,  $X$  contains samples and  $Y$  contains class labels.

**Output:** updated model  $f$  after this training epoch

**Process:**

**for** Batch data  $X$  and  $Y$  in  $S$  **do**

Run model  $f$  to classify the samples and divide the samples into two groups, wrongly-classified  $X_0, Y_0$  and correctly-classified  $X_1, Y_1$  where  $X = X_0 \cup X_1$  and  $Y = Y_0 \cup Y_1$

Get noisy samples  $X_n = BPGD(X_1, Y_1, \mathcal{E}(X_1))$  and classify them  $\hat{Y}_n = f(X_n) \cdot \mathcal{E}(X_1)$  is a sub-array of  $\mathcal{E}$ , containing the estimated margins of samples in  $X_1$ .  $BPGD$  is described in Algorithm 3.

Compute the loss  $L$ :

$L_0 = \text{cross\_entropy}(f(X_0), Y_0)$  (take sum)

$L_1 = \text{cross\_entropy}(f(X_1), Y_1)$  (take sum)

$L_2 = \text{cross\_entropy}(f(X_n), Y_1)$  (take sum)

$L = ((1 - \beta) \cdot (L_0 + L_1) + \beta \cdot L_2) / \text{batch\_size}$

Back-propagate from  $L$  and update the model  $f$

**end for**

---

training samples have different magnitudes (i.e., vector norms). The rationale for doing so is discussed in section 2.3. Here, the margin of a sample is the minimum distance between the sample and the decision boundaries. It is difficult to compute the exact margin for a sample in a high dimension space, and therefore we can only estimate it.

We developed Algorithm 3, named BPGD, to find noisy samples on decision boundaries. At the very beginning of the IMA training process, the margins of the training samples are initialized to a small number equal to margin expansion step size in Algorithm 2. Intuitively, during IMA training, the margin of a training sample keeps increasing as if a ball is expanding (the ball center is the sample  $x$ , and the radius is the margin  $\mathcal{E}(x)$ ; it is called  $\varepsilon$ -ball), until the ball of the sample  $x$  collides with the ball of another sample  $x'$  in a different class. When the two balls collide and therefore a local decision boundary is formed, Algorithm 2 will prevent them from further expansion by refining/shrinking margins (Fig. 4). In section 2.3, we will show that an equilibrium state may exist (Fig. 5) under which the margins of the samples are maximized.

## 2.3 the Equilibrium State

We can show that on certain conditions, an equilibrium state (Fig. 5-Left) exists under which the margins of the samples are maximized. To simplify the discussion, we assume there are three classes and three decision boundaries between classes (Fig. 5-Right). The softmax output of the neural network model

---

**Algorithm 2** update margin estimation after an epoch

---

**Input:**  $S = (x, y)$  is the training set.  $f$  is the DNN model and  $\hat{y} = f(x)$ .  $\mathcal{E}$  is an array of the estimated margins of training samples.  $\mathcal{E}(x)$  is the estimated margin of  $x$ .  $\Delta_\varepsilon$  is margin expansion step size.  $\varepsilon_{max}$  is the maximum noise level, i.e., the allowed maximum margin.

**Output:** updated  $\mathcal{E}$

**Process:**

**for** each sample  $x$  and  $y$  in  $S$  **do**

    Get noisy sample  $x_n = BPGD(x, y, \mathcal{E}(x))$  (From Algorithm 1)

**if**  $x_n$  is on decision boundary (not None, which means  $\mathcal{E}(x)$  is larger than what it should be) **then**

        Update  $\mathcal{E}(x) = (\|x - x_n\|_p + \mathcal{E}(x))/2$  (shrink)

**else**

        Update  $\mathcal{E}(x) = \mathcal{E}(x) + \Delta_\varepsilon$  (expand)

**end if**

**end for**

Clip every element of  $\mathcal{E}$  into the range of 0 to  $\varepsilon_{max}$

**Note:** Every  $\mathcal{E}(x)$  is initialized to be  $\Delta_\varepsilon$  which can be set to  $\varepsilon_{max}$  divided by the number of adversarial training epochs. The algorithm runs in mini-batches.

---

$f$  has three components:  $P_1$ ,  $P_2$  and  $P_3$  corresponding to the three classes. If a point (i.e., a sample)  $x$  is on the decision boundary  $B_{ij}$  between class- $i$  ( $c_i$ ) and class- $j$  ( $c_j$ ), then  $P_i(x) = P_j(x)$ . The mathematical expectation of the cross-entropy loss of the noisy samples ( $L_2$  in Algorithm 1) is:

$$E = \mathbf{E}_{X_n \in c_1} (-\log(P_1(X_n))) + \mathbf{E}_{X_n \in c_2} (-\log(P_2(X_n))) + \mathbf{E}_{X_n \in c_3} (-\log(P_3(X_n))) \quad (3)$$

The IMA method puts the noisy samples on the decision boundaries, thus:

$$\mathbf{E}_{X_n \in c_1} (-\log(P_1(X_n))) = \mathbf{E}_{X_n \in c_1, B_{12}} (-\log(P_1(X_n))) + \mathbf{E}_{X_n \in c_1, B_{13}} (-\log(P_1(X_n))) \quad (4)$$

$$\mathbf{E}_{X_n \in c_2} (-\log(P_2(X_n))) = \mathbf{E}_{X_n \in c_2, B_{12}} (-\log(P_2(X_n))) + \mathbf{E}_{X_n \in c_2, B_{23}} (-\log(P_2(X_n))) \quad (5)$$

$$\mathbf{E}_{X_n \in c_3} (-\log(P_3(X_n))) = \mathbf{E}_{X_n \in c_3, B_{13}} (-\log(P_3(X_n))) + \mathbf{E}_{X_n \in c_3, B_{23}} (-\log(P_3(X_n))) \quad (6)$$

If the noisy samples (random variables)  $X_n \in c_i$  and  $X_n \in c_j$  have the same spatial distribution on the decision boundary  $B_{ij}$  between the two classes, Eq.(3) can be simplified to

$$E = E_{X_n \in B_{12}} + E_{X_n \in B_{23}} + E_{X_n \in B_{13}} \quad (7)$$

---

**Algorithm 3** (BPGD): generate noisy samples

---

**Input:** a sample  $x$  with class label  $y$ , the estimated margin  $\varepsilon$  of  $x$ , and the model  $f \cdot N_{PGD}$  is the number of iterations in PGD.  $N_{binary}$  is the number of iterations in binary search.

**Output:**  $x_n = BPGD(x, y, \varepsilon)$

**Process:**

Run the standard  $PGD(x, y, \varepsilon)$  and obtain a sequence of noisy samples ( $N_{PGD}$  samples)

Classify those noisy samples using the model  $f$

**if** all of the noisy samples are correctly-classified (case-0 in Fig.2) **then**

**return** None ( $x_n$  is None and will be ignored)

**else**

    (case-1 in Fig.2) Find  $x_{n1}$  and  $x_{n2}$ , two adjacent samples in the sequence.  $x_{n1}$  is correctly-classified and  $x_{n2}$  is wrongly-classified. Thus,  $x_{n1}$  and  $x_{n2}$  are close to the decision boundary.

    Run binary search along the straight-line segment between  $x_{n1}$  and  $x_{n2}$  in order to find  $x_n$  on the decision boundary (Fig. 3)

**return**  $x_n$

**end if**

**Note:** 1. It is unnecessary to store the whole sequence. The algorithm runs in mini-batches. 2.  $N_{binary}$  is set to 10, which is constant. So, this binary search's time complexity is  $O(1)$ .

---

where

$$\begin{aligned} E_{X_n \in B_{ij}} &= \mathbf{E}_{X_n \in B_{ij}} (-\log(P_i(X_n)) - \log(P_j(X_n))) \\ &= \mathbf{E}_{X_n \in B_{ij}} (-\log(P_i(X_n)P_j(X_n))) \\ &\geq \mathbf{E}_{X_n \in B_{ij}} \left( -\log \left( \frac{P_i(X_n) + P_j(X_n)}{2} \right)^2 \right) \end{aligned} \tag{8}$$

$E$  reaches the minimum when  $P_i(X_n) = P_j(X_n)$ .

The analysis shows that the loss of noisy samples will increase if the decision boundaries of the model  $f$  change from the current state. Thus, when the loss ( $L_0 + L_1$ ) on clean data is minimized and noisy samples are generated on the decision boundaries, an equilibrium is reached under the condition that noisy samples have the same spatial distribution on the decision boundaries between classes. This analysis provides the rationale that our IMA method puts the noisy/adversarial samples on decision boundaries as much as possible, which is significantly different from the theory of the MMA method [Ding et al.(2020)Ding, Sharma, Lui, and Huang].



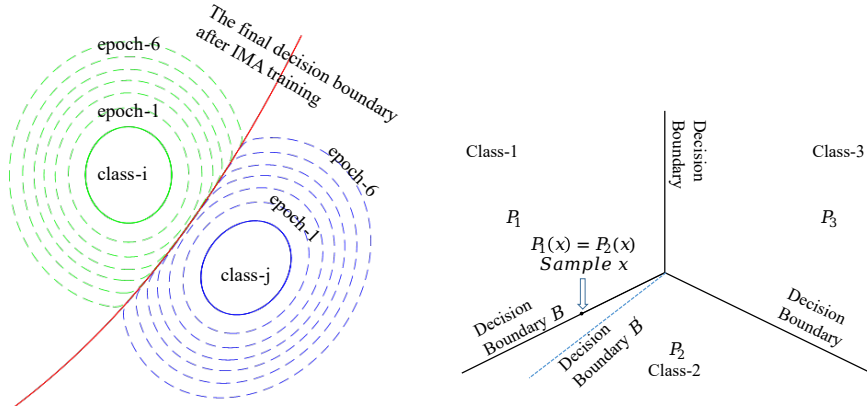


Figure 5: Left: Equilibrium State; Right: Three-class Scenario.

### 3 Experiments of Image Classification

We applied the IMA method on classification for 5 DNNs on 5 different datasets: Moons, Fashion-MNIST, SVHN, CIFAR10 and COVID-19 CT. To describe the DNNs, we use “COV (a, b, c, d, e)” to represent a convolution layer with “a” input channels, “b” output channels, kernel size of “c”, stride of “d” and padding of “e”; “Linear (f, g)” to denote a linear layer with input size of “f” and output size of “g”; “IN” to denote instance normalization; “LN” to denote layer normalization, and “LR” to denote leaky ReLU.

To obtain the baseline performance, each DNN was trained with cross-entropy loss on clean data, denoted by “ce”. To evaluate the performance, we compared our method with other adversarial training methods, including: (1) 20-PGD ( $N_{PGD}=20$  and  $\alpha=4$ ) based vanilla adversarial training with noise level  $\varepsilon$ , denoted by “adv  $\varepsilon$ ” [Goodfellow et al.(2015)Goodfellow, Shlens, and Szegedy, Kurakin et al.(2016)Kurakin, Goodfellow, Bengio, et al.] ; (2) TRADES in [Zhang et al.(2019)Zhang, Yu, Jiao, Xing, El Ghaoui, and Jordan]; (3) MMA in [Ding et al.(2020)Ding, Sharma, Lui, and Huang]; (4) DDN in [Rony et al.(2019)Rony, Hafemann, Oliveira, Ayed, Sabourin, and Granger]; (5) FAT in [Zhang et al.(2020)Zhang, Xu, Han, Niu, Cui, Sugiyama, and Kankanhalli]; (6) GAIRAT in [Zhang et al.(2021)Zhang, Zhu, Niu, Han, Sugiyama, and Kankanhalli]. MMA is a state-of-the-art method, and TRADES was state-of-the-art at the time of its publication.  $N_{PGD}$  of IMA is 20. We used PGD to evaluate the robustness of the methods, which is widely used for method evaluation [Liao et al.(2018)Liao, Liang, Dong, Pang, Hu, and Zhu, Uesato et al.(2018)Uesato, O’donoghue, Kohli, and Oord]. The number of PGD iterations is 100 to ensure a strong attack, and it is called 100-PGD. To further enhance the stability of testing result, each 100-PGD runs twice using MarginalLoss and CrossEntropyLoss respectively, which is implemented in [Ding et al.(2019)Ding, Wang, and Jin]. For simplicity, we use “**clean accuracy**” to refer to the accuracy on clean data,

and “noisy accuracy” to refer to the accuracy on noisy data. The details of the experiments are in Appendix. G. Because of the nature of IMA, it does not have significant robust overfitting problem [Rice et al.(2020)Rice, Wong, and Kolter, Kim et al.(2021)Kim, Lee, and Lee] (see Appendix H.1). Blackbox-attack evaluation with SPSA [Uesato et al.(2018)Uesato, O’donoghue, Kohli, and Oord] is in Appendix H.2, which shows there is no gradient obfuscation in IMA.

### 3.1 Evaluation on Moons dataset

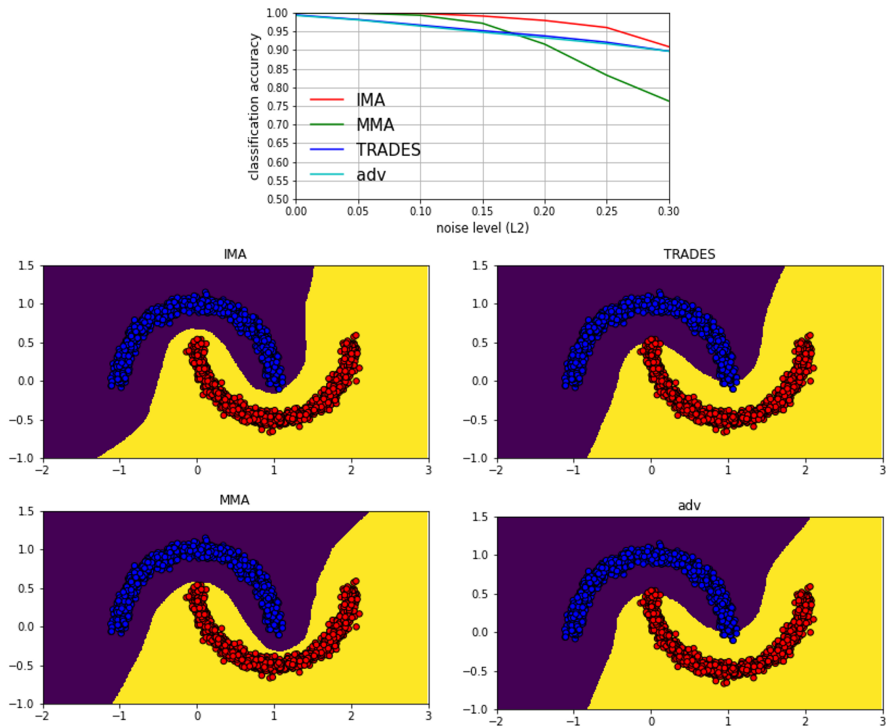


Figure 6: Results on Moons dataset (L2 norm in 100-PGD).

The Moons dataset is available in sk-learn [Pedregosa et al.(2011)Pedregosa, Varoquaux, Gramfort, Michel, Thirion, Grisel, Blondel, Prettenhofer, Weiss, Dubourg, et al.]. There are two classes of 2D points in the dataset. The training set has 20000 samples, the validation set has 2000 samples, and the test set has 2000 samples. The neural network structure is Linear(2, 32)-LR-Linear(32, 64)-LN-LR-Linear(64, 128)-LN-LR-Linear(128, 2). The purpose of this evaluation is to visualize the decision boundaries of the models trained by different adversarial training methods. To measure robustness on the test set, adversarial samples on different noise levels (defined by L2 norm) are generated by the 100-PGD. From Fig. 6, our method IMA is better than the other methods, and its decision

Table 1: Classification accuracy on Fashion-MNIST (L2 norm in 100-PGD).

Noise	0.0	0.5	1.0	2.0	3.0
ce	91.17	25.12	0.33	0.0	0.0
IMA	88.98	80.73	69.64	47.62	32.42
MMA	89.26	80.70	69.27	46.17	26.51
FAT	86.09	79.08	67.21	34.82	10.79
GAIRAT	83.11	69.53	53.24	20.41	2.15
DDN	86.21	78.53	68.80	49.47	34.67
TRADES	91.76	61.03	49.77	34.25	18.75
adv1.0	90.86	80.96	65.49	27.26	5.13
adv3.0	91.72	64.10	58.59	47.54	33.25
adv5.0	91.48	48.51	41.61	30.11	21.21

boundary is close to the “middle line” of the two classes. The results of TRADES and adv0.3 are very similar: the decision boundary is far away from most of the red dots. We note that 0.3 is roughly the distance between two classes.

### 3.2 Evaluation on Fashion-MNIST, SVHN and CIFAR10 datasets

Table 2: Classification accuracy on SVHN (L2 norm in 100-PGD).

Noise	0.0	0.1	0.25	0.5	1.0
ce	93.20	75.88	41.25	11.85	0.92
IMA	89.69	85.01	76.82	60.50	31.90
MMA	87.65	83.22	75.18	59.74	32.15
FAT	88.01	81.94	70.24	42.76	12.12
GAIRAT	91.66	84.90	68.25	36.52	7.31
DDN	86.95	82.17	73.85	58.43	31.40
TRADES	87.30	80.76	69.03	45.81	12.38
adv0.5	89.86	84.90	75.08	53.90	20.62
adv1.0	87.30	82.84	75.04	58.87	26.54
adv2.0	86.63	81.75	71.95	54.58	28.83

We used Fashion-MNIST dataset [Xiao et al.(2017)Xiao, Rasul, and Vollgraf] instead of MNIST which is too easy. The dataset contains  $28 \times 28$  grayscale images in 10 classes (shirts, shoes, etc.). The network structure is COV(1, 64, 5, 2, 2)-LR-COV(64, 128, 5, 2, 2)-IN-LR-COV (128, 256, 5, 2, 2)-IN-LR-COV (256, 512, 4, 1, 0)-Flatten-LN-LR-Linear(512, 10). The results are shown in Table. 1. IMA outperformed MMA, FAT, and GAIRAT. DDN performed slightly better than IMA on the noise levels of 2.0 and 3.0, but it had a lower clean accuracy.

We note that clean accuracy should not be sacrificed too much in order to achieve high robustness (i.e., noisy accuracy). “adv  $\varepsilon$ ” is very sensitive to the parameter  $\varepsilon$ .

We also used SVHN dataset which contains  $32 \times 32$  color images of 0  $\sim$  9 digits[Netzer et al.(2011)Netzer, Wang, Coates, Bissacco, Wu, and Ng]. The network structure is COV(3, 32, 3, 1, 1)-LR-COV(32, 32, 3, 2, 1)-IN-LR-COV(32, 64, 3, 1, 1)-IN-LR-Conv2d(64, 64, 3, 2, 1)-IN-LR-COV(64, 128, 3, 1, 1)-IN-LR-Conv2d(128, 128, 3, 2, 1)-IN-LR-COV(128, 256, 4, 1, 0)-Flatten-LN-LR-Linear(256, 10). The results are shown in Table. 2. IMA outperformed all the other methods.

Table 3: Classification accuracy on CIFAR10 (L2 norm in 100-PGD).

Noise	0.0	0.5	1.0	1.5
ce	94.92	0.98	0.0	0.0
IMA	88.22	65.82	39.80	20.50
MMA	88.02	66.19	37.80	15.61
FAT	87.11	52.02	15.89	3.01
GAIRAT	86.75	49.49	16.35	3.45
DDN	89.05	66.51	39.02	16.63
TRADES	84.98	54.61	21.48	6.23
adv0.5	89.10	65.61	33.23	11.29
adv1.0	83.25	66.69	46.11	26.16
adv1.5	75.80	62.74	48.35	33.80

Then, we used CIFAR10 dataset which contains 60000  $32 \times 32$  color images in 10 classes[Krizhevsky et al.(2009)Krizhevsky, Hinton, et al.]. The network is WRN-28-4[Ding et al.(2020)Ding, Sharma, Lui, and Huang]. The results are shown in Table. 3. IMA outperformed MMA, FAT, GAIRAT, and TRADES. DDN performed slightly better than IMA on the noise levels of 0 and 0.5. DDN uses 100 iterations to find adversarial samples, which is almost equivalent to using 100-PGD for adversarial training, and this is the reason that DDN performed better on this dataset. In contrast, IMA uses 20-PGD internally, which has a much smaller computation cost. “adv  $\varepsilon$ ” is very sensitive to the parameter  $\varepsilon$ .

### 3.3 the Effect of $\varepsilon_{max}$ in the IMA

$\varepsilon_{max}$  is the maximum noise level for training. This parameter needs to be tuned in almost every adversarial training method. From Table 6, Table 4 and Table 5, we can see that, in general, a larger  $\varepsilon_{max}$  leads to a higher accuracy on noisy data. However, unlike vanilla adversarial training (see Table 8) and MMA (see Table 7), IMA with a larger  $\varepsilon_{max}$  does not have a significant decrease in the accuracy on clean data. This is further discussed in Appendix C.

Table 4: Effect of  $\varepsilon_{max}$  in IMA on Fashion-MNIST test set (L2 norm-defined noise level,  $\Delta\varepsilon = 5/60$ ).

noise	0	0.5	1	2	3
$\varepsilon_{max} = 3.0$	89.40	80.98	70.34	48.07	28.34
$\varepsilon_{max} = 4.0$	88.81	80.23	69.07	46.99	31.47
$\varepsilon_{max} = 5.0$	88.98	80.73	69.64	47.62	32.42
$\varepsilon_{max} = 6.0$	88.90	80.68	69.64	47.74	32.92
$\varepsilon_{max} = 7.0$	88.57	79.55	67.74	46.80	33.27

Table 5: Effect of  $\varepsilon_{max}$  in IMA on SVHN test set (L2 norm-defined noise level,  $\Delta\varepsilon = 2/60$ ).

noise	0	0.1	0.25	0.5	1.0
$\varepsilon_{max} = 1.0$	90.53	86.16	77.76	59.63	27.20
$\varepsilon_{max} = 1.5$	89.75	85.50	77.29	60.34	30.30
$\varepsilon_{max} = 2.0$	89.69	85.01	76.82	60.50	31.90
$\varepsilon_{max} = 2.5$	89.96	85.51	77.50	60.53	31.44
$\varepsilon_{max} = 3.0$	89.97	85.80	77.31	60.49	31.57
$\varepsilon_{max} = 3.5$	90.00	85.57	77.49	60.38	31.37
$\varepsilon_{max} = 4.0$	89.42	85.16	77.07	60.41	31.58
$\varepsilon_{max} = 4.5$	89.79	85.45	77.20	60.31	31.89

### 3.4 Application of COVID-19 detection from CT images

We used a public COVID-19 CT image dataset [Soares et al.(2020)Soares, Angelov, Biaso, Froes, and Abe], which was collected from patients in hospitals from Sao Paulo, Brazil. It contains 1252 CT scans (2D images) that are positive for COVID-19 infection and 1230 CT scans (2D images) for patients non-infected by COVID-19, 2482 CT scans in total. From infected cases, we randomly selected 200 samples for testing, 30 for validation, and 1022 for training. From the uninfected cases, we randomly selected 200 for testing, 30 for validation and 1000 for training. Each image is resized to  $224 \times 224$ . Since there is no pixel segmentation mask in the dataset, we can only perform classification for COVID-19 detection on the image level. We modified the output layer of the Resnet-18 model [He et al.(2016)He, Zhang, Ren, and Sun] for the binary classification task: uninfected (label 0) vs infected (label 1), and we also replaced batch normalization with instance normalization because it is known that batch normalization is not stable for small batch-size [Wu & He(2018)Wu and He]. As shown in the previous studies [Shi et al.(2020)Shi, Wang, Shi, Wu, Wang, Tang, He, Shi, and Shen], infected regions in the images have a special pattern called ground-glass opacity.

Details of this experiment can be seen in Appendix G. To measure robustness on the test set, adversarial samples on different noise levels (L2 norm) are

Table 6: Effect of  $\varepsilon_{max}$  in IMA on CIFAR10 test set (L2 norm-defined noise level,  $\Delta\varepsilon = 3/100$ ).

noise	0	0.5	1.0	1.5
$\varepsilon_{max} = 1.0$	89.35	65.30	37.08	17.73
$\varepsilon_{max} = 2.0$	88.21	66.28	40.86	22.50
$\varepsilon_{max} = 3.0$	88.07	66.13	41.07	23.09

Table 7: Effect of  $\varepsilon_{max}$  in MMA on CIFAR10 test set (L2 norm-defined noise level).

noise	0	0.5	1.0	1.5
$\varepsilon_{max} = 1.0$	88.02	66.19	37.80	15.61
$\varepsilon_{max} = 2.0$	84.22	65.98	46.11	28.56
$\varepsilon_{max} = 3.0$	82.11	64.25	47.61	33.48

generated by the 100-PGD. From Table. 25, the results show that no single method performed the best on all noise levels. IMA and “adv 10” had very similar performance, and IMA performed better than MMA.

Fig. 7 shows the distribution of estimated margins of all the training samples, where x-axis shows the magnitude of margins (in L2 norm) and y-axis shows the frequency. From Fig. 7 (right), it can be seen that about 1/6 of the estimated margins from MMA are larger than 30, which means about 1/6 of samples should have been free of influence of noises with magnitude less than 30. However, the accuracy of MMA on the noise level of 30 is 0. The results show that MMA significantly overestimated the margins of samples because MMA does not consider the equilibrium (Fig.5) between classes. From Fig. 7 (left), the problem of margin overestimation was relieved in IMA, which is the reason that IMA outperforms MMA in all the evaluations in this paper. It also can be seen that the vanilla adversarial training (“adv  $\varepsilon$ ”) is good when the training noise level  $\varepsilon$  is chosen “properly”. A straightforward way to find a good  $\varepsilon$  would be running grid-research and evaluating the performance on the validation set, which is computationally expensive. The margin distribution (Fig. 7(left)) estimated by our method IMA indicates a good  $\varepsilon = 10$  for vanilla adversarial training. This is because 10 is just smaller than the majority of the margins, which will not make the noisy samples to go cross the true decision boundary.

## 4 Extension of IMA for Medical Image Segmentation

The IMA algorithm can also be applied to improve DNN robustness for image segmentation tasks. For image segmentation tasks, we reformulate a segmen-

Table 8: Effect of  $\varepsilon_{max}$  in vanilla adversarial training on CIFAR10 test set (L2 norm-defined noise level).

noise	0	0.5	1.0	1.5
$\varepsilon_{max} = 1.0$	83.25	66.69	46.11	26.16
$\varepsilon_{max} = 2.0$	71.05	59.80	47.92	35.39

Table 9: Classification accuracy on COVID-19 CT image dataset (L2 norm in 100-PGD).

Noise	0	1	3	5	10	30
ce	95.75	9.98	0.0	0.0	0.0	0.0
IMA	91.25	90.25	87.75	83.25	57.00	0.0
MMA	89.00	88.50	84.25	80.00	57.50	0.0
DDN	90.25	88.50	84.75	78.75	59.75	0.0
TRADES	97.25	12.75	10.25	11.00	19.75	48.75
GAIRAT	92.50	88.25	72.50	50.25	12.50	0.0
FAT	90.00	88.00	81.50	64.25	16.00	0.0
adv10	93.50	92.25	89.50	83.50	53.50	0.0
adv20	95.25	25.50	20.00	21.50	22.50	3.00
adv30	85.25	6.25	1.50	2.00	5.00	23.00

tation task as a classification task. Since Dice index is often used to evaluate segmentation performance, a segmentation can be considered “correct” if Dice  $>$  a threshold, and “wrong” otherwise, which is binary classification to classify the segmentation output. In the experiments, this Dice threshold is set to 60% for all of the datasets because a Dice score higher than 60% is considered “good” for medical applications[Visser et al.(2020)Visser, Petr, Müller, Eijgelaar, Hendriks, Witte, Barkhof, van Herk, Mutsaerts, Vrenken, et al., Visser et al.(2019)Visser, Müller, van Duijn, Smits, Verburg, Hendriks, Nabuurs, Bot, Eijgelaar, Witte, et al., Cicchetti(1994), Bartko(1991)]. For non-medical images, there is no consensus about a good Dice score, which is the reason we used medical images.

In the experiments, we applied the IMA method on a self-configuring DNN, named nnUnet [Isensee et al.(2021)Isensee, Jaeger, Kohl, Petersen, and Maier-Hein]. The nnUnet can automatically configure itself, including preprocessing, network architecture, training, and post-processing for the input dataset. In the experiment, we selected three publically available datasets [Isensee et al.(2021)Isensee, Jaeger, Kohl, Petersen, and Maier-Hein], which are Heart (D2), Hippocampus (D4) and Prostate (D5)[Simpson et al.(2019)Simpson, Antonelli, Bakas, Bilello, Farahani, Van Ginneken, Kopp-Schneider, Landman, Litjens, Menze, et al.]. Noise levels are measured by L2 norm. Because image segmentation robustness is an underexplored area, we compared only three methods: (1) the proposed IMA, denoted by “IMA”; (2) the 20-PGD based vanilla

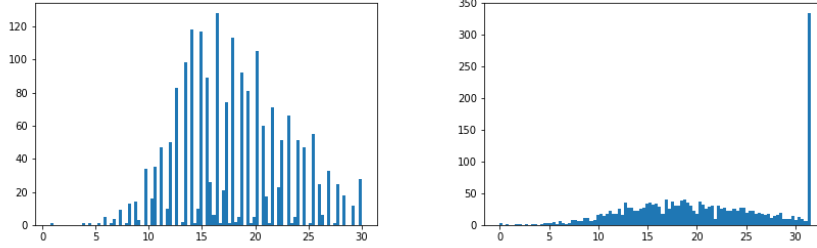


Figure 7: IMA estimated margin distribution (left), and MMA estimated margin distribution (right). MMA significantly overestimated the margins.

adversarial training with training noise level of  $\varepsilon$ , denoted by “adv  $\varepsilon$ ” [Goodfellow et al.(2015)Goodfellow, Shlens, and Szegedy] ; (3) the nnUnet, which is trained on clean data, denoted by “nnUnet”. For evaluation, the adversarial attack is 100-PGD. For these methods, we used the original loss function in [Isensee et al.(2021)Isensee, Jaeger, Kohl, Petersen, and Maier-Hein] as the replacement of cross-entropy loss. The details are in Appendix G.

In the experiments, two metrics are used to evaluate the performance. The first one is “Total Voxel Dice Index (TVDI)” and the second one is “Average Dice Index (ADI)”. The definitions of these two metrics are in Appendix I.

Table 10: D2: Total Voxel Dice Index.

Noise	0	5	15	25
nnUnet	92.46	69.12	2.01	0.0
IMA	85.34	80.23	69.34	56.33
adv5	87.23	80.78	60.12	35.01
adv15	84.21	80.15	67.48	50.98
adv25	80.44	76.11	68.19	58.90

Table 11: D2: Average Dice Index.

Noise	0	5	15	25
nnUnet	80.01	51.69	2.17	0.0
IMA	75.43	70.16	55.79	44.06
adv5	75.12	65.43	46.31	23.78
adv15	72.15	66.34	53.36	38.12
adv25	66.78	61.65	52.67	43.79



## 4.1 Evaluation on Heart (D2)

This dataset has 20 labeled 3D images: 16 for training, 1 for validation and 3 for testing. The median shape of each 3D image is  $115 \times 320 \times 232$ , where 115 is the number of slices. In this experiment, we only focused on 2D segmentation, so each slice is an input sample of the model. The batch size (40), patch size ( $320 \times 256$ ) and network structure are self-configured by nnUnet for this dataset. From Table. 10, “nnUnet” has the weakest defense against adversarial attack, whose TVDI score drops to almost 0 at the noise level of 15. It can be seen that “adv5” has a high clean TVDI (0.87), but is not robust enough (its TVDI score drops very fast as the noise level goes up). “adv25” is very robust as its TVDI score drops slowliest when the noise level goes up), but its clean TVDI score is more than 10% lower than the score of the original “nnUnet”, which means the noise level for training is so large that it has significantly affected the original model’s functionality. “adv15” is not as robust as “IMA” in general. The results show the weakness of vanilla adversarial training: very large training noise will destroy the model while very small training noise cannot make the model robust enough. As revealed by the AVI metric (Table. 11), IMA has a significantly better performance than the other methods.

## 4.2 Evaluation on Hippocampus (D4)

Table 12: D4: Total Voxel Dice Index.

Noise	0	1	5	10	15
nnUnet	86.45	78.13	15.00	0.0	0.0
IMA	82.19	80.14	72.49	56.27	32.01
adv1	85.36	82.01	60.89	20.98	2.03
adv5	83.21	81.90	70.68	50.79	19.98
adv15	79.89	78.11	69.56	50.67	27.76

Table 13: D4: Average Dice Index.

Noise	0	1	5	10	15
nnUnet	75.23	64.10	9.00	0.0	0.0
IMA	74.01	72.06	64.32	49.11	26.95
adv1	73.95	69.05	48.83	15.04	0.91
adv5	70.56	69.05	58.16	37.85	16.17
adv15	69.23	66.80	58.23	41.12	22.49

This D4 dataset has 260 labeled 3D images: 208 for training, 17 for validation

and 35 for testing. The median shape of each 3D image is  $36 \times 50 \times 35$ , where 36 is the number of slices and  $50 \times 35$  is the input size. The batch size (366), patch size ( $56 \times 40$ ) and network structure are self-configured by nnUnet for this dataset. From Table. 12, “nnUnet”’s TVDI score drops to almost 0 at the noise level of 10, which shows the 100-PGD is a very strong attack. It can be seen that “adv1” has a good clean TVDI score (85%), but is not robust enough. “adv15” is very robust but has the lowest clean TVDI score ( $< 80\%$ ). “adv5” has a very high TVDI score on clean data but is not as robust as “IMA”. As revealed by the ADI metric in Fig. 13, IMA has the best performance.

### 4.3 Evaluation on Prostate (D5)

Table 14: D5: Total Voxel Dice Index.

Noise	0	10	20	40
nnUnet	80.89	37.14	18.09	7.01
IMA	72.23	66.14	59.15	43.45
adv40	70.76	63.18	54.67	38.13
adv20	72.46	65.34	56.78	38.19
adv10	73.12	61.67	50.43	28.23

Table 15: D5: Average Dice Index.

Noise	0	10	20	40
nnUnet	74.34	30.14	13.90	4.08
IMA	66.80	61.15	55.41	38.01
adv40	65.49	56.13	45.78	28.90
adv20	65.89	56.34	44.76	27.86
adv10	66.04	54.48	39.96	21.85

This D5 dataset has 32 labeled 3D images: 25 for training, 2 for validation and 5 for testing. The median shape of each 3D image is  $20 \times 320 \times 319$ , where 20 is the number of slices and  $320 \times 319$  is the input size. The batch size (32), patch size ( $320 \times 320$ ) and network structure are self-configured by nnUnet for this dataset. As shown in Table. 14, although the clean TVDI scores of “IMA”, “adv20” and “adv10” are almost the same (around 0.73), “adv20” and “adv10” are not as robust as “IMA”. Also, “adv40” is not as good as “IMA” on both clean and noisy data. As shown by the ADI metric in Table. 15, IMA has the best performance.

## 5 Conclusion

In this study, we proposed a novel Increasing-Margin Adversarial (IMA) training method to improve the robustness of DNNs for image classification and segmentation tasks. Our method aims to increase the margins of the training samples gradually to improve DNN robustness against adversarial attacks. The experiment results show that our method IMA outperformed other comparing methods in general and significantly improved DNN classification accuracy on noisy data while keeping a high accuracy on clean data. Also, the experiment results show that our method can be applied to improve DNN robustness for image segmentation tasks. We hope our approach may facilitate the development of robust DNNs for more medical applications in the future.

## References

- [Agarwal et al.(2021)Agarwal, Vatsa, and Singh] Agarwal, A., Vatsa, M., and Singh, R. Role of optimizer on network fine-tuning for adversarial robustness (student abstract). In *AAAI*, pp. 15745–15746. AAAI Press, 2021. URL <https://ojs.aaai.org/index.php/AAAI/article/view/17869>.
- [Ai et al.(2020)Ai, Yang, Hou, Zhan, Chen, Lv, Tao, Sun, and Xia] Ai, T., Yang, Z., Hou, H., Zhan, C., Chen, C., Lv, W., Tao, Q., Sun, Z., and Xia, L. Correlation of chest ct and rt-pcr testing in coronavirus disease 2019 (covid-19) in china: a report of 1014 cases. *Radiology*, pp. 200642, 2020.
- [Akhtar & Mian(2018)Akhtar and Mian] Akhtar, N. and Mian, A. Threat of adversarial attacks on deep learning in computer vision: A survey. *IEEE Access*, 6:14410–14430, 2018.
- [Athalye et al.(2018)Athalye, Carlini, and Wagner] Athalye, A., Carlini, N., and Wagner, D. Obfuscated gradients give a false sense of security: Circumventing defenses to adversarial examples. In Dy, J. and Krause, A. (eds.), *ICML*, volume 80 of *Proceedings of Machine Learning Research*, pp. 274–283. PMLR, 10–15 Jul 2018. URL <https://proceedings.mlr.press/v80/athalye18a.html>.
- [Awasthi et al.(2021)Awasthi, Yu, Ferng, Tomkins, and Juan] Awasthi, P., Yu, G., Ferng, C.-S., Tomkins, A., and Juan, D.-C. Adversarial robustness across representation spaces. In *Proceedings of the IEEE/CVF Conference on Computer Vision and Pattern Recognition*, pp. 7608–7616, 2021.
- [Bartko(1991)] Bartko, J. J. Measurement and reliability: statistical thinking considerations. *Schizophrenia bulletin*, 17(3):483–489, 1991.
- [Bui et al.(2021)Bui, Le, Zhao, Montague, de Vel, Abraham, and Phung] Bui, T., Le, T., Zhao, H., Montague, P., de Vel, O. Y., Abraham, T., and Phung,

- D. Improving ensemble robustness by collaboratively promoting and demoting adversarial robustness. In *AAAI*, pp. 6831–6839. AAAI Press, 2021. URL <https://ojs.aaai.org/index.php/AAAI/article/view/16843>.
- [Carlini & Wagner(2017)Carlini and Wagner] Carlini, N. and Wagner, D. Towards evaluating the robustness of neural networks. In *2017 IEEE Symposium on Security and Privacy (SP)*, pp. 39–57. IEEE, 2017.
- [Cazenavette et al.(2021)Cazenavette, Murdock, and Lucey] Cazenavette, G., Murdock, C., and Lucey, S. Architectural adversarial robustness: The case for deep pursuit. In *Proceedings of the IEEE/CVF Conference on Computer Vision and Pattern Recognition*, pp. 7150–7158, 2021.
- [Chen et al.(2021)Chen, Kung, and Chen] Chen, P.-C., Kung, B.-H., and Chen, J.-C. Class-aware robust adversarial training for object detection. In *Proceedings of the IEEE/CVF Conference on Computer Vision and Pattern Recognition*, pp. 10420–10429, 2021.
- [Chen et al.(2017)Chen, Zhang, Sharma, Yi, and Hsieh] Chen, P.-Y., Zhang, H., Sharma, Y., Yi, J., and Hsieh, C.-J. Zoo: Zeroth order optimization based black-box attacks to deep neural networks without training substitute models. In *Proceedings of the 10th ACM workshop on artificial intelligence and security*, pp. 15–26, 2017.
- [Cheng et al.(2020)Cheng, Lei, Chen, Dhillon, and Hsieh] Cheng, M., Lei, Q., Chen, P.-Y., Dhillon, I., and Hsieh, C.-J. Cat: Customized adversarial training for improved robustness, 2020.
- [Cicchetti(1994)] Cicchetti, D. V. Guidelines, criteria, and rules of thumb for evaluating normed and standardized assessment instruments in psychology. *Psychological assessment*, 6(4):284, 1994.
- [Deng et al.(2021)Deng, Yang, Xu, Su, and Zhu] Deng, Z., Yang, X., Xu, S., Su, H., and Zhu, J. Libre: A practical bayesian approach to adversarial detection. In *Proceedings of the IEEE/CVF Conference on Computer Vision and Pattern Recognition*, pp. 972–982, 2021.
- [Ding et al.(2019)Ding, Wang, and Jin] Ding, G. W., Wang, L., and Jin, X. AdverTorch v0.1: An adversarial robustness toolbox based on pytorch, 2019.
- [Ding et al.(2020)Ding, Sharma, Lui, and Huang] Ding, G. W., Sharma, Y., Lui, K. Y. C., and Huang, R. Mma training: Direct input space margin maximization through adversarial training. In *ICLR*, 2020.
- [Elliott et al.(2021)Elliott, Law, and Russell] Elliott, A., Law, S., and Russell, C. Explaining classifiers using adversarial perturbations on the perceptual ball. In *Proceedings of the IEEE/CVF Conference on Computer Vision and Pattern Recognition*, pp. 10693–10702, 2021.

- [Eykholt et al.(2018)Eykholt, Evtimov, Fernandes, Li, Rahmati, Xiao, Prakash, Kohno, and Song] Eykholt, K., Evtimov, I., Fernandes, E., Li, B., Rahmati, A., Xiao, C., Prakash, A., Kohno, T., and Song, D. Robust physical-world attacks on deep learning visual classification. In *CVPR*, pp. 1625–1634, 2018.
- [Fan & Li(2021)Fan and Li] Fan, J. and Li, W. Adversarial training and provable robustness: A tale of two objectives. In *AAAI*, pp. 7367–7376. AAAI Press, 2021. URL <https://ojs.aaai.org/index.php/AAAI/article/view/16904>.
- [Gokhale et al.(2021)Gokhale, Anirudh, Kailkhura, Thiagarajan, Baral, and Yang] Gokhale, T., Anirudh, R., Kailkhura, B., Thiagarajan, J. J., Baral, C., and Yang, Y. Attribute-guided adversarial training for robustness to natural perturbations. In *AAAI*, pp. 7574–7582. AAAI Press, 2021. URL <https://ojs.aaai.org/index.php/AAAI/article/view/16927>.
- [Gong et al.(2021)Gong, Ren, Ye, and Liu] Gong, C., Ren, T., Ye, M., and Liu, Q. Maxup: Lightweight adversarial training with data augmentation improves neural network training. In *Proceedings of the IEEE/CVF Conference on Computer Vision and Pattern Recognition*, pp. 2474–2483, 2021.
- [Goodfellow et al.(2015)Goodfellow, Shlens, and Szegedy] Goodfellow, I., Shlens, J., and Szegedy, C. Explaining and harnessing adversarial examples. In *ICLR*, 2015. URL <http://arxiv.org/abs/1412.6572>.
- [Graese et al.(2016)Graese, Rozsa, and Boulton] Graese, A., Rozsa, A., and Boulton, T. E. Assessing threat of adversarial examples on deep neural networks. In *ICMLA*, pp. 69–74. IEEE, 2016.
- [He et al.(2016)He, Zhang, Ren, and Sun] He, K., Zhang, X., Ren, S., and Sun, J. Deep residual learning for image recognition. In *CVPR*, pp. 770–778, 2016.
- [Ilyas et al.(2018)Ilyas, Engstrom, Athalye, and Lin] Ilyas, A., Engstrom, L., Athalye, A., and Lin, J. Black-box adversarial attacks with limited queries and information. In *ICML*, pp. 2137–2146. PMLR, 2018.
- [Isensee et al.(2021)Isensee, Jaeger, Kohl, Petersen, and Maier-Hein] Isensee, F., Jaeger, P. F., Kohl, S. A., Petersen, J., and Maier-Hein, K. H. nnu-net: a self-configuring method for deep learning-based biomedical image segmentation. *Nature methods*, 18(2):203–211, 2021.
- [Jia et al.(2021a)Jia, Cao, and Gong] Jia, J., Cao, X., and Gong, N. Z. Intrinsic certified robustness of bagging against data poisoning attacks. In *AAAI*, pp. 7961–7969. AAAI Press, 2021a. URL <https://ojs.aaai.org/index.php/AAAI/article/view/16971>.
- [Jia et al.(2021b)Jia, Song, Ma, and Yang] Jia, S., Song, Y., Ma, C., and Yang, X. Iou attack: Towards temporally coherent black-box adversarial attack

- for visual object tracking. In *Proceedings of the IEEE/CVF Conference on Computer Vision and Pattern Recognition*, pp. 6709–6718, 2021b.
- [Kim et al.(2021)Kim, Lee, and Lee] Kim, H., Lee, W., and Lee, J. Understanding catastrophic overfitting in single-step adversarial training. In *AAAI*, 2021.
- [Krizhevsky et al.(2009)Krizhevsky, Hinton, et al.] Krizhevsky, A., Hinton, G., et al. Learning multiple layers of features from tiny images. 2009.
- [Kurakin et al.(2016)Kurakin, Goodfellow, Bengio, et al.] Kurakin, A., Goodfellow, I., Bengio, S., et al. Adversarial examples in the physical world, 2016.
- [Li et al.(2021)Li, Li, Pan, and Zhu] Li, X., Li, X., Pan, D., and Zhu, D. Improving adversarial robustness via probabilistically compact loss with logit constraints. In *AAAI*, pp. 8482–8490. AAAI Press, 2021. URL <https://ojs.aaai.org/index.php/AAAI/article/view/17030>.
- [Liang & Huang(2021)Liang and Huang] Liang, Y. and Huang, D. Large norms of CNN layers do not hurt adversarial robustness. In *AAAI*, pp. 8565–8573. AAAI Press, 2021. URL <https://ojs.aaai.org/index.php/AAAI/article/view/17039>.
- [Liao et al.(2018)Liao, Liang, Dong, Pang, Hu, and Zhu] Liao, F., Liang, M., Dong, Y., Pang, T., Hu, X., and Zhu, J. Defense against adversarial attacks using high-level representation guided denoiser. In *CVPR*, pp. 1778–1787, 2018.
- [Madry et al.(2018)Madry, Makelov, Schmidt, Tsipras, and Vladu] Madry, A., Makelov, A., Schmidt, L., Tsipras, D., and Vladu, A. Towards deep learning models resistant to adversarial attacks. In *ICLR*, 2018.
- [Mirjalili & Ross(2017)Mirjalili and Ross] Mirjalili, V. and Ross, A. Soft biometric privacy: Retaining biometric utility of face images while perturbing gender. In *IJCB*, pp. 564–573. IEEE, 2017.
- [Miyato et al.(2018)Miyato, Maeda, Koyama, and Ishii] Miyato, T., Maeda, S.-i., Koyama, M., and Ishii, S. Virtual adversarial training: a regularization method for supervised and semi-supervised learning. *IEEE transactions on pattern analysis and machine intelligence*, 41(8):1979–1993, 2018.
- [Netzer et al.(2011)Netzer, Wang, Coates, Bissacco, Wu, and Ng] Netzer, Y., Wang, T., Coates, A., Bissacco, A., Wu, B., and Ng, A. Y. Reading digits in natural images with unsupervised feature learning. In *NIPS Workshop on Deep Learning and Unsupervised Feature Learning*, 2011.
- [Ning et al.(2021)Ning, Tao, Chen, and Huang] Ning, K., Tao, L., Chen, S., and Huang, S. Improving model robustness by adaptively correcting perturbation levels with active queries. In *AAAI*, pp. 9161–9169. AAAI Press, 2021. URL <https://ojs.aaai.org/index.php/AAAI/article/view/17106>.

- [Paszke et al.(2017)Paszke, Gross, Chintala, Chanan, Yang, DeVito, Lin, Desmaison, Antiga, and Lerer] Paszke, A., Gross, S., Chintala, S., Chanan, G., Yang, E., DeVito, Z., Lin, Z., Desmaison, A., Antiga, L., and Lerer, A. Automatic differentiation in pytorch. 2017.
- [Pedregosa et al.(2011)Pedregosa, Varoquaux, Gramfort, Michel, Thirion, Grisel, Blondel, Prettenhofer, Weiss, Pedregosa, F., Varoquaux, G., Gramfort, A., Michel, V., Thirion, B., Grisel, O., Blondel, M., Prettenhofer, P., Weiss, R., Dubourg, V., et al. Scikit-learn: Machine learning in python. *the Journal of machine Learning research*, 12:2825–2830, 2011.
- [Rampini et al.(2021)Rampini, Pestarini, Cosmo, Melzi, and Rodola] Rampini, A., Pestarini, F., Cosmo, L., Melzi, S., and Rodola, E. Universal spectral adversarial attacks for deformable shapes. In *Proceedings of the IEEE/CVF Conference on Computer Vision and Pattern Recognition*, pp. 3216–3226, 2021.
- [Rice et al.(2020)Rice, Wong, and Kolter] Rice, L., Wong, E., and Kolter, Z. Overfitting in adversarially robust deep learning. In *ICML*, pp. 8093–8104. PMLR, 2020.
- [Rony et al.(2019)Rony, Hafemann, Oliveira, Ayed, Sabourin, and Granger] Rony, J., Hafemann, L. G., Oliveira, L. S., Ayed, I. B., Sabourin, R., and Granger, E. Decoupling direction and norm for efficient gradient-based l2 adversarial attacks and defenses. In *Proceedings of the IEEE/CVF Conference on Computer Vision and Pattern Recognition*, pp. 4322–4330, 2019.
- [Ruoss et al.(2021)Ruoss, Baader, Balunovic, and Vechev] Ruoss, A., Baader, M., Balunovic, M., and Vechev, M. T. Efficient certification of spatial robustness. In *AAAI*, pp. 2504–2513. AAAI Press, 2021. URL <https://ojs.aaai.org/index.php/AAAI/article/view/16352>.
- [Sarkar et al.(2021)Sarkar, Sarkar, and Balasubramanian] Sarkar, A., Sarkar, A., and Balasubramanian, V. N. Enhanced regularizers for attributional robustness. In *AAAI*, pp. 2532–2540. AAAI Press, 2021. URL <https://ojs.aaai.org/index.php/AAAI/article/view/16355>.
- [Shi et al.(2020)Shi, Wang, Shi, Wu, Wang, Tang, He, Shi, and Shen] Shi, F., Wang, J., Shi, J., Wu, Z., Wang, Q., Tang, Z., He, K., Shi, Y., and Shen, D. Review of artificial intelligence techniques in imaging data acquisition, segmentation and diagnosis for covid-19. *IEEE reviews in biomedical engineering*, 2020.
- [Simpson et al.(2019)Simpson, Antonelli, Bakas, Bilello, Farahani, Van Ginneken, Kopp-Schneider, Landman, Simpson, A. L., Antonelli, M., Bakas, S., Bilello, M., Farahani, K., Van Ginneken, B., Kopp-Schneider, A., Landman, B. A., Litjens, G., Menze, B., et al. A large annotated medical image dataset for the development and evaluation of segmentation algorithms, 2019.

- [Soares et al.(2020)Soares, Angelov, Biaso, Froes, and Abe] Soares, E., Angelov, P., Biaso, S., Froes, M. H., and Abe, D. K. Sars-cov-2 ct-scan dataset: A large dataset of real patients ct scans for sars-cov-2 identification. *medRxiv*, 2020.
- [Szegedy et al.(2013)Szegedy, Zaremba, Sutskever, Bruna, Erhan, Goodfellow, and Fergus] Szegedy, C., Zaremba, W., Sutskever, I., Bruna, J., Erhan, D., Goodfellow, I., and Fergus, R. Intriguing properties of neural networks, 2013.
- [Tramer et al.(2020)Tramer, Carlini, Brendel, and Madry] Tramer, F., Carlini, N., Brendel, W., and Madry, A. On adaptive attacks to adversarial example defenses. In *NeurIPS*, 2020.
- [Uesato et al.(2018)Uesato, O’donoghue, Kohli, and Oord] Uesato, J., O’donoghue, B., Kohli, P., and Oord, A. Adversarial risk and the dangers of evaluating against weak attacks. In *ICML*, pp. 5025–5034. PMLR, 2018.
- [Visser et al.(2019)Visser, Müller, van Duijn, Smits, Verburg, Hendriks, Nabuurs, Bot, Eijgelaar, Witte, et al.] Visser, M., Müller, D., van Duijn, R., Smits, M., Verburg, N., Hendriks, E., Nabuurs, R., Bot, J., Eijgelaar, R., Witte, M., et al. Inter-rater agreement in glioma segmentations on longitudinal mri. *NeuroImage: Clinical*, 22: 101727, 2019.
- [Visser et al.(2020)Visser, Petr, Müller, Eijgelaar, Hendriks, Witte, Barkhof, van Herk, Mutsaerts, Vrenken, et al.] Visser, M., Petr, J., Müller, D. M., Eijgelaar, R. S., Hendriks, E. J., Witte, M., Barkhof, F., van Herk, M., Mutsaerts, H. J., Vrenken, H., et al. Accurate mr image registration to anatomical reference space for diffuse glioma. *Frontiers in neuroscience*, 14:585, 2020.
- [Wang & Yu(2019)Wang and Yu] Wang, H. and Yu, C.-N. A direct approach to robust deep learning using adversarial networks. In *ICLR*, 2019.
- [Wang et al.(2021)Wang, He, Peng, Shao, Yang, Zhou, and Hogg] Wang, H., He, F., Peng, Z., Shao, T., Yang, Y.-L., Zhou, K., and Hogg, D. Understanding the robustness of skeleton-based action recognition under adversarial attack. In *Proceedings of the IEEE/CVF Conference on Computer Vision and Pattern Recognition*, pp. 14656–14665, 2021.
- [Wang et al.(2008)Wang, Lu, Liang, Eremina, Zhang, Wang, Chen, and Manzione] Wang, J., Lu, H., Liang, Z., Eremina, D., Zhang, G., Wang, S., Chen, J., and Manzione, J. An experimental study on the noise properties of x-ray ct sinogram data in radon space. *Physics in Medicine & Biology*, 53(12):3327, 2008.
- [Wang & He(2021)Wang and He] Wang, X. and He, K. Enhancing the transferability of adversarial attacks through variance tuning. In *Proceedings of the IEEE/CVF Conference on Computer Vision and Pattern Recognition*, pp. 1924–1933, 2021.



- [Wang et al.(2020)Wang, Zou, Yi, Bailey, Ma, and Gu] Wang, Y., Zou, D., Yi, J., Bailey, J., Ma, X., and Gu, Q. Improving adversarial robustness requires revisiting misclassified examples. In *ICLR*, 2020.
- [WHO(2020)] WHO. Coronavirus disease (covid-19) dashboard(<https://covid19.who.int/>). 2020.
- [Wu et al.(2021a)Wu, Liu, Huang, Wang, and Lin] Wu, T., Liu, Z., Huang, Q., Wang, Y., and Lin, D. Adversarial robustness under long-tailed distribution. In *Proceedings of the IEEE/CVF Conference on Computer Vision and Pattern Recognition*, pp. 8659–8668, 2021a.
- [Wu et al.(2021b)Wu, Su, Lyu, and King] Wu, W., Su, Y., Lyu, M. R., and King, I. Improving the transferability of adversarial samples with adversarial transformations. In *Proceedings of the IEEE/CVF Conference on Computer Vision and Pattern Recognition*, pp. 9024–9033, 2021b.
- [Wu & He(2018)Wu and He] Wu, Y. and He, K. Group normalization. In *ECCV*, pp. 3–19, 2018.
- [Xiao et al.(2017)Xiao, Rasul, and Vollgraf] Xiao, H., Rasul, K., and Vollgraf, R. Fashion-mnist: a novel image dataset for benchmarking machine learning algorithms, 2017.
- [Yang et al.(2021)Yang, Guo, Wang, and Xu] Yang, S., Guo, T., Wang, Y., and Xu, C. Adversarial robustness through disentangled representations. In *AAAI*, pp. 3145–3153. AAAI Press, 2021. URL <https://ojs.aaai.org/index.php/AAAI/article/view/16424>.
- [Yu et al.(2021)Yu, Gao, and Xu] Yu, Y., Gao, X., and Xu, C.-Z. Lafeat: Piercing through adversarial defenses with latent features. In *Proceedings of the IEEE/CVF Conference on Computer Vision and Pattern Recognition*, pp. 5735–5745, 2021.
- [Zhang et al.(2019)Zhang, Yu, Jiao, Xing, El Ghaoui, and Jordan] Zhang, H., Yu, Y., Jiao, J., Xing, E., El Ghaoui, L., and Jordan, M. Theoretically principled trade-off between robustness and accuracy. In *ICML*, pp. 7472–7482. PMLR, 2019.
- [Zhang et al.(2020)Zhang, Xu, Han, Niu, Cui, Sugiyama, and Kankanhalli] Zhang, J., Xu, X., Han, B., Niu, G., Cui, L., Sugiyama, M., and Kankanhalli, M. Attacks which do not kill training make adversarial learning stronger. In *ICML*, pp. 11278–11287. PMLR, 2020.
- [Zhang et al.(2021)Zhang, Zhu, Niu, Han, Sugiyama, and Kankanhalli] Zhang, J., Zhu, J., Niu, G., Han, B., Sugiyama, M., and Kankanhalli, M. Geometry-aware instance-reweighted adversarial training. In *ICLR*, 2021.

**Appendix A** further discusses the necessity of adversarial robustness. Appendix B discusses the effect of parameter  $\beta$  in the IMA. Appendix C discusses the effect of  $\varepsilon_{max}$  in the IMA. Appendix D discusses the trade-off between robustness and accuracy. Appendix E further discusses the equilibrium state. Appendix F shows some examples of the clean and noisy images used in the experiment of the main paper. Appendix G shows the training details in the experiments in the main paper. Appendix H shows some additional results, including black-box attack evaluation and robust overfitting situation of IMA. Appendix I shows the definition of TVDI and ADI.

## A Adversarial Robustness is Essential

It seems that adversarial noises are created by algorithms (e.g. PGD) and therefore it is only a security issue caused by hackers. In fact, random imaging noises could also be “adversarial” noises leading to wrong classifications. For the COVID-19 application, we did an additional test and found out that 2.75% of the noisy samples with uniform white noises on the level of 0.05, can cause the model “ce” to make wrong classifications. 2.75% is not a negligible number for this application. We note that CT imaging noises can be better described by Poisson distribution [Wang et al.(2008)Wang, Lu, Liang, Eremina, Zhang, Wang, Chen, and Manzione]. However, without the hardware parameters of the CT machine, it is impossible to simulate Poisson noises. Nevertheless, adversarial robustness should be the built-in property of a model for this application, and all of the DNN models in the previous COVID-19 studies [Shi et al.(2020)Shi, Wang, Shi, Wu, Wang, Tang, He, Shi, and Shen] should be checked and enhanced for adversarial robustness before deploying those models in clinics and hospitals.

## B the Effect of $\beta$ in the IMA

We evaluated the effect of  $\beta$  in the IMA method on the Fashion-MNIST dataset, and the other settings are the same as those in the corresponding Section in the main paper (e.g. white-box 100-PGD attack on the test set). The results are reported in Table 16.

Table 16: Results on Fashion-MNIST (L2 norm-defined noise level)

noise	0	0.5	1	2	3
$\beta = 0.1$	89.46	79.95	67.59	43.29	28.27
$\beta = 0.3$	89.00	79.87	67.96	45.82	30.90
$\beta = 0.5$	88.98	80.73	69.64	47.62	32.42
$\beta = 0.7$	87.78	80.86	70.73	47.64	32.64
$\beta = 0.9$	86.82	80.74	72.16	50.96	33.51

It can be clearly seen that smaller  $\beta$  leads to higher accuracy on clean data (noise level = 0) and larger  $\beta$  leads to higher accuracy on noisy data.

**The trade-off between robustness and accuracy is highly nonlinear**, as shown in Table 17: a small decrease in accuracy on clean data can result in a large increase in accuracy on noisy data.

Table 17: Accuracy differences caused by different values of  $\beta$

noise	0	0.5	1	2	3
$\beta = 0.1$	89.46	79.95	67.59	43.29	28.27
$\beta = 0.5$	88.98	80.73	69.64	47.62	32.42
difference	0.48	0.78	2.05	4.33	4.15

**The nonlinear trade-off between robustness and accuracy makes it difficult to directly compare two methods, as different methods make different trade-offs between robustness and accuracy.** The average accuracy is clearly not a good measure of performance on robustness. Adjusting the parameter  $\beta$  of IMA is not a computationally efficient approach to make a trade-off between robustness and accuracy, because for every possible value of  $\beta$  in the range of 0 to 1, the user has to train a model from scratch through many epochs. In Appendix C, we show that the user of IMA can make such a trade-off much more efficiently by “adjusting” the parameter  $\varepsilon_{max}$  of IMA.

## C the Effect of $\varepsilon_{max}$ in the IMA

In this appendix, we show how  $\varepsilon_{max}$  in Algorithm 2 affects the performance of IMA, and how to choose its value.  $\varepsilon_{max}$  is the allowed maximum margin of the samples in IMA. And, it is the maximum noise level for training, which exists in almost every adversarial training method.

### C.1 the Effect of $\varepsilon_{max}$

From Table 18, Table 19 and Table 20, we can see that, in general, a larger  $\varepsilon_{max}$  leads to a higher accuracy on noisy data. However, unlike vanilla adversarial training (see Table 22) and MMA (see Table 21), IMA with a larger  $\varepsilon_{max}$  does not have a significant decrease in the accuracy on clean data. This is because adversarial samples generated by IMA are of good quality and are not likely to cross over the true decision boundary and mislead the model (note: if an adversarial sample goes across the true decision boundary, then its true class label is changed, which means the class label of this adversarial sample is wrong during training ). We can also see that, if  $\varepsilon_{max}$  is too small, the accuracy on noisy data with large noises decreases, which is because the sample margins are not allowed to expand sufficiently. After the  $\varepsilon_{max}$  reaches a specific noise level (4.0 for Fashion-MNIST, 1.5 for SVHN), the accuracy on noisy data will

no longer change significantly as  $\varepsilon_{max}$  increases, which is because the sample margins have been expanded sufficiently large. Thus, for IMA, the user only needs to avoid setting  $\varepsilon_{max}$  to a too-small value. A very large  $\varepsilon_{max}$  is not likely to significantly harm the accuracy on clean data. As a comparison (see Table 22 and Table 21), for MMA, a large  $\varepsilon_{max}$  will lead to a significant decrease in accuracy on clean data, which is not good for real applications.

Table 18: Effect of  $\varepsilon_{max}$  in IMA on Fashion-MNIST test set (L2 norm-defined noise level,  $\Delta\varepsilon = 5/60$ ).

noise	0	0.5	1	2	3
$\varepsilon_{max} = 3.0$	89.40	80.98	70.34	48.07	28.34
$\varepsilon_{max} = 4.0$	88.81	80.23	69.07	46.99	31.47
$\varepsilon_{max} = 5.0$	88.98	80.73	69.64	47.62	32.42
$\varepsilon_{max} = 6.0$	88.90	80.68	69.64	47.74	32.92
$\varepsilon_{max} = 7.0$	88.57	79.55	67.74	46.80	33.27

Table 19: Effect of  $\varepsilon_{max}$  in IMA on SVHN test set (L2 norm-defined noise level,  $\Delta\varepsilon = 2/60$ ).

noise	0	0.1	0.25	0.5	1.0
$\varepsilon_{max} = 1.0$	90.53	86.16	77.76	59.63	27.20
$\varepsilon_{max} = 1.5$	89.75	85.50	77.29	60.34	30.30
$\varepsilon_{max} = 2.0$	89.69	85.01	76.82	60.50	31.90
$\varepsilon_{max} = 2.5$	89.96	85.51	77.50	60.53	31.44
$\varepsilon_{max} = 3.0$	89.97	85.80	77.31	60.49	31.57
$\varepsilon_{max} = 3.5$	90.00	85.57	77.49	60.38	31.37
$\varepsilon_{max} = 4.0$	89.42	85.16	77.07	60.41	31.58
$\varepsilon_{max} = 4.5$	89.79	85.45	77.20	60.31	31.89

Table 20: Effect of  $\varepsilon_{max}$  in IMA on CIFAR10 test set (L2 norm-defined noise level,  $\Delta\varepsilon = 3/100$ ).

noise	0	0.5	1.0	1.5
$\varepsilon_{max} = 1.0$	89.35	65.30	37.08	17.73
$\varepsilon_{max} = 2.0$	88.21	66.28	40.86	22.50
$\varepsilon_{max} = 3.0$	88.07	66.13	41.07	23.09

Table 21: Effect of  $\varepsilon_{max}$  in MMA on CIFAR10 test set (L2 norm-defined noise level).

noise	0	0.5	1.0	1.5
$\varepsilon_{max} = 1.0$	88.02	66.19	37.80	15.61
$\varepsilon_{max} = 2.0$	84.22	65.98	46.11	28.56
$\varepsilon_{max} = 3.0$	82.11	64.25	47.61	33.48

Table 22: Effect of  $\varepsilon_{max}$  in vanilla adversarial training on CIFAR10 test set (L2 norm-defined noise level).

noise	0	0.5	1.0	1.5
$\varepsilon_{max} = 1.0$	83.25	66.69	46.11	26.16
$\varepsilon_{max} = 2.0$	71.05	59.80	47.92	35.39

## C.2 How to Choose $\varepsilon_{max}$

Noisy samples with adversarial noises can be correctly classified by humans but may be incorrectly classified by neural networks, which is basically the definition of adversarial noises. By following this definition, we choose the allowed maximum margin by looking at the noisy samples: if the noise magnitude is too large such that we barely can recognize the objects in the images, then this magnitude is chosen as the allowed maximum margin. This is how we choose the allowed maximum margin in the experiments on the datasets.

Next, we provide a strategy for the user of IMA to refine the choice of  $\varepsilon_{max}$  by making a trade-off between robustness and accuracy. As shown in Fig. 8, the trade-off between clean-accuracy (i.e., accuracy on clean data) and robustness (i.e., accuracy on noisy data) can be observed during training by using our IMA method.

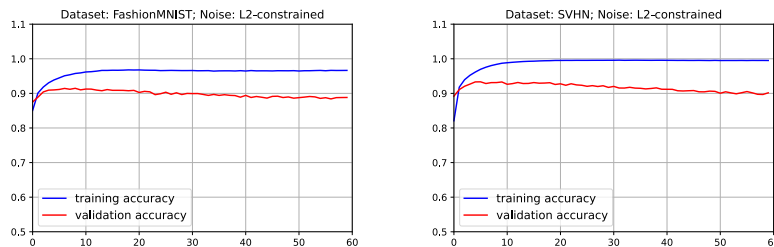


Figure 8: The training and validation curves (accuracy vs epoch) on different datasets obtained by using our IMA method. The accuracy scores are measured on clean data.

During IMA training, the (estimated) margin of a sample  $x_1$  in class-1 is initialized to be close to 0 and it keeps increasing as if the radius of a ball increases during the training process. The sample  $x_1$  is at the center of the ball, and the radius of the ball is the current margin of the sample. When the ball of  $x_1$  collides with the ball of another sample  $x_2$  from a different class-2, then a local decision boundary is formed, and the two balls stop expanding.

If there are enough training data samples, a sample  $x$  in some class will eventually meet with its counterpart in another class somewhere in the middle of the two classes, which forms a robust decision boundary. In practice, the amount of training data is never enough to cover the input space, and therefore the margin of a sample could be overestimated because of missing the counterparts that are needed to stop the expansion of the margin. If the margins of many samples are overestimated, then the balls of these samples may penetrate the true decision boundary and cause lower classification accuracy on the validation set of clean samples, **which explains the existence of the trade-off between robustness and clean-accuracy from the perspective of sample margins.**

The above analysis is confirmed by the trend of the training and validation accuracy curves in Fig. 8: after some epochs, the training accuracy curve becomes stable, and the validation accuracy curve starts to decrease, which indicates margin overestimation occurs. **For our IMA method, the cause of margin overestimation is the lack of data in high dimensional space.** In the 2D Moons dataset, there are enough training samples, and therefore, the decision boundary of our IMA method is almost in the “middle” between the two classes, i.e., no margin overestimation.

**Using the validation accuracy curve, the user of IMA can choose the allowed maximum margin** such that validation accuracy is above a pre-defined threshold that is set by the user to meet some application requirements. Next, we demonstrate this approach on the Fashion-MNIST dataset. We note that during IMA training, the margins of the samples are gradually increasing. Immediately after  $M$  epochs, the possible maximum of the training sample margins is  $M \times \Delta\varepsilon$  where  $\Delta\varepsilon$  is the margin expansion step size in Algorithm 2. Thus, the maximum margin is  $\varepsilon_{max} = M \times \Delta\varepsilon$  for the model trained for  $M$  epochs. Since we do not know the threshold on validation accuracy, which a user may be interested in on the dataset, we selected six models trained by IMA after 10, 20, 30, 40, 50, and 60 epochs, and we evaluated the robustness of the six models on the test set by using the 100-PGD attack. Basically, we re-analyzed the models trained through 60 epochs. The results are reported in Table 23, which reveals the effect of  $\varepsilon_{max}$  on robustness.

Table 23: Effect of  $\varepsilon_{max}$  on Fashion-MNIST test set (L2 norm-defined noise level,  $\Delta\varepsilon = 5/60$ ).

noise	0	0.5	1	2	3	0 (Validation)
$\varepsilon_{max} = 10\Delta\varepsilon$	91.59	76.43	52.74	11.46	0.28	91.43
$\varepsilon_{max} = 20\Delta\varepsilon$	90.91	80.91	66.72	34.08	8.27	90.87
$\varepsilon_{max} = 30\Delta\varepsilon$	89.89	81.34	69.85	44.16	20.58	89.93
$\varepsilon_{max} = 40\Delta\varepsilon$	89.61	81.32	70.15	46.65	26.66	89.38
$\varepsilon_{max} = 50\Delta\varepsilon$	89.11	81.04	70.17	47.43	29.95	89.08
$\varepsilon_{max} = 60\Delta\varepsilon$	88.98	80.73	69.64	47.62	32.42	88.61

Table 24: Effect of  $\varepsilon_{max}$  on SVHN test set (L2 norm-defined noise level,  $\Delta\varepsilon = 2/60$ ).

noise	0	0.1	0.25	0.5	1.0	0 (Validation)
$\varepsilon_{max} = 10\Delta\varepsilon$	93.45	88.12	74.67	45.33	10.84	93.05
$\varepsilon_{max} = 20\Delta\varepsilon$	92.70	88.36	78.80	56.86	20.59	92.83
$\varepsilon_{max} = 30\Delta\varepsilon$	92.34	88.34	79.51	59.92	25.57	91.96
$\varepsilon_{max} = 40\Delta\varepsilon$	91.47	87.33	78.82	60.98	28.45	91.26
$\varepsilon_{max} = 50\Delta\varepsilon$	90.62	86.46	78.10	60.66	29.16	90.80
$\varepsilon_{max} = 60\Delta\varepsilon$	89.69	85.01	76.82	60.50	31.90	90.17

From Table 23, it can be clearly seen that smaller  $\varepsilon_{max}$  leads to higher accuracy on clean data (noise level = 0), and larger  $\varepsilon_{max}$  leads to higher accuracy on noisy data. Since the maximum of the sample margins gradually increases during IMA training, the validation accuracy changes gradually (increasing and then decreasing), which makes it easy for the user of our method to choose the trained model with validation accuracy above the user-defined threshold.

We have done similar analyses on the models trained by IMA through 60 epochs on the SVHN dataset. We selected six models trained by IMA after 10, 20, 30, 40, 50, and 60 epochs, and we evaluated the robustness of the six models on the test set by using the 100-PGD attack. The results are reported in Table 24, which reveal the effect of  $\varepsilon_{max}$  on robustness. By monitoring the validation accuracy curve during training, the user of IMA can choose a trained model such that validation accuracy of the chosen model is above a threshold defined by the user to meet some application requirements.

### C.3 COVID-19 application

Next, we plot the curves from the COVID-19 dataset in Fig. 9. The validation accuracy decreased only slightly after 20 epochs, which means the value of the allowed maximum margin is reasonable and the risk of margin overestimation is low.

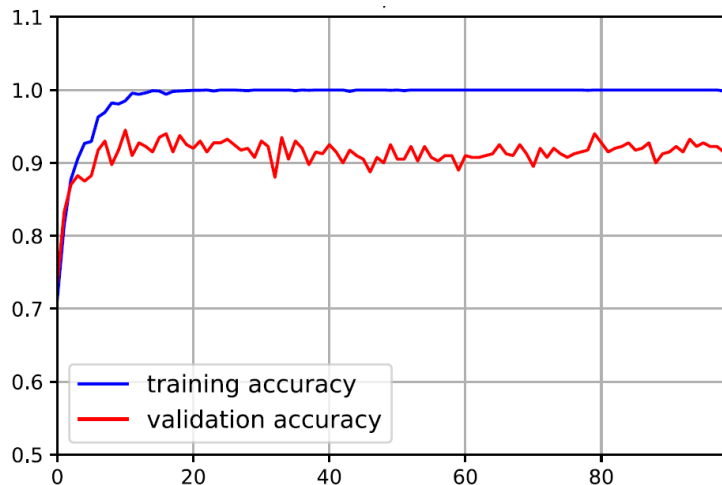


Figure 9: The training and validation curves (accuracy vs epoch) on the COVID-19 CT dataset obtained by using our IMA method. The accuracy scores are measured on clean data.

We note that using the margin distribution estimated by IMA, we can obtain a good perturbation magnitude  $\varepsilon$  (10) for the vanilla adversarial training. When  $\varepsilon=10$ , vanilla adversarial training achieved the best performance on the COVID-19 CT dataset, when the noise level is smaller than 5. Please see Fig. 10 which contains the margin distribution estimated by IMA. In practice, we only need robustness against noises within a certain level, because significantly noisy images can only be produced from a malfunctioning CT machine. Thus, vanilla adversarial training (denoted by  $\text{adv } \varepsilon$ ) should be good enough (much less computation cost and time compared to advanced adversarial training methods) as long as its parameter  $\varepsilon$  is appropriate. In this application, the good value of  $\varepsilon$  is 10, as revealed by the margin distribution estimated by IMA.



Table 25: Classification accuracy on COVID-19 CT image dataset (L2 norm in 100-PGD).

Noise	0	1	3	5	10	30
ce	95.75	9.98	0.0	0.0	0.0	0.0
IMA	91.25	90.25	87.75	83.25	57.00	0.0
MMA	89.00	88.50	84.25	80.00	57.50	0.0
DDN	90.25	88.50	84.75	78.75	59.75	0.0
TRADES	97.25	12.75	10.25	11.00	19.75	48.75
GAIRAT	92.50	88.25	72.50	50.25	12.50	0.0
FAT	90.00	88.00	81.50	64.25	16.00	0.0
adv10	93.50	92.25	89.50	83.50	53.50	0.0
adv20	95.25	25.50	20.00	21.50	22.50	3.00
adv30	85.25	6.25	1.50	2.00	5.00	23.00

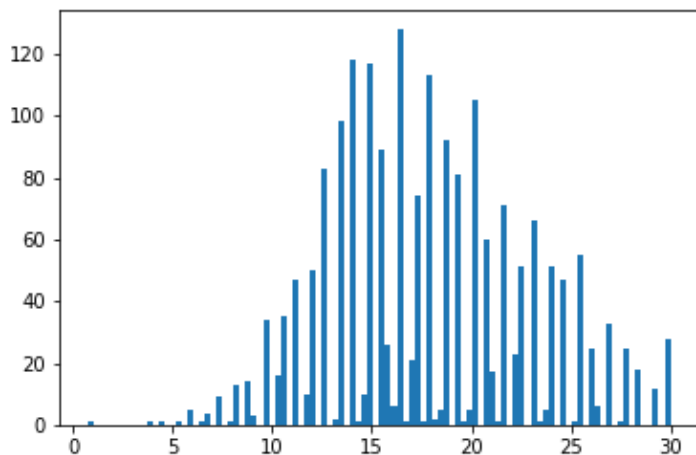


Figure 10: Margin distribution estimated by IMA on training set

For vanilla adversarial training, a straightforward way to find a good  $\varepsilon$  would be running grid research and evaluating the performance on the validation set. However, the grid-research in a large range (e.g. 0 to 30) is impractical because adversarial training is computationally expensive and time-consuming, compared to standard training with cross-entropy loss and clean data. The margin distribution estimated by IMA can reveal a good range of the  $\varepsilon$ , and then grid-research in this small range can be performed to find the optimal  $\varepsilon$ . After the optimal  $\varepsilon$  is found for vanilla adversarial training, we could combine other techniques to further improve robustness.

## D Trade-off Between Robustness and Accuracy: Sample Margins’ Perspective

In this appendix, we discuss the trade-off between robustness and accuracy from the perspective of sample margins. Let  $x$  denote a clean sample (i.e., unaltered by any adversarial attacks). Let  $x_{(\delta)}$  denote the noisy sample generated by adding an adversarial noise  $\delta$  to  $x$ , i.e.,  $x_{(\delta)} = x + \delta$ . The vector norm of  $\delta$  is  $\varepsilon$ . Let  $y$  denote the true class label of  $x$ .

For vanilla adversarial training, the class label of the noisy sample  $x_{(\delta)}$  is assumed to be the same as the class label  $y$  of the clean sample  $x$ , no matter how large the noise level  $\varepsilon$  is. This label assignment can be wrong if  $\varepsilon$  is very large: large enough such that  $x_{(\delta)}$  may “look like” a sample in a different class (not  $y$ ), which has been shown in numerous studies. Here, “look like” refers to the judgment of a human. However, it is impractical to let a person actually look at every noisy sample to assign the right label to it.

If there are unlimited training samples that cover the input space, the samples can reveal the true class distributions  $p(x|y)$ . Then, the true decision boundary can be obtained by Bayesian classification using  $p(x|y)$  and  $p(y)$  of each of the classes. For example,  $p(x|y)$  can be simply modeled by a Gaussian mixture model, and  $p(y)$  may be assumed to be the same for every class. If we assume Bayesian classification with unlimited data is as good as the judgment of human experts, then Bayesian decision boundary is the most robust against noises. Let  $g(x)$  denote the Bayesian classifier ( $g$  means ground truth), and it outputs the true label of the input:  $y = g(x)$  and  $y_{(\delta)} = g(x_{(\delta)})$ . Using the Bayesian-optimal decision boundary, the true margin of a clean sample  $x$  can be obtained, i.e., the (minimum) distance between  $x$  and the decision boundary, which is denoted by  $m(x)$ .

During adversarial training (vanilla or IMA), a noisy sample is generated,  $x_{(\delta)} = x + \delta$  with  $\varepsilon = \|\delta\|$ , and the class label  $y$  is assigned to it. If the noise/perturbation magnitude  $\varepsilon$  is larger than the true margin  $m(x)$ , then the assigned class label is wrong for  $x_{(\delta)}$ , and training the model with  $x_{(\delta)}$  may cause its decision boundary to deviate from the Bayesian-optimal decision boundary even if the model  $f(x)$  is initialized to be very close to  $g(x)$ . As a result, the classification accuracy on the test/validation set (clean data) will become lower, but the classification accuracy on the training set (clean data) may not change because the decision boundary has been pushed far away from the clean training sample  $x$ . **This phenomenon has been revealed by the training and validation accuracy curves of IMA (see Fig. 8), which explains the well-known trade-off between robustness and accuracy.**

Thus, the success of adversarial training depends on the accurate estimation of the true margin  $m(x)$ : if  $\mathcal{E}(x) = m(x)$ , then IMA could be perfect. For the 2D Moons dataset, IMA can indeed find a nearly perfect decision boundary, significantly better than the other methods (see Fig. 6).

However, for a high dimensional dataset (e.g. Fashion-MNIST), there are not enough training samples to cover the input space. As a result, perfect

Bayesian classification is not achievable because of inaccurate estimation of  $p(x|y)$ , and IMA cannot obtain perfect estimations of the true margins because there may not exist the counterparts in other classes (not  $y$ ) that can stop the expansion of  $\varepsilon$ -ball (margin estimation) of  $x$  in class  $y$ . Margin overestimation is revealed by the gradually-decreasing trend of the validation accuracy curve (see Fig. 8). However, the good news for the user of IMA is that the user can choose a good value of  $\varepsilon_{max}$  such that the validation accuracy is above a pre-defined threshold (e.g. 90% for the COVID-19 application). Also, the user does not need to pre-define the value of  $\varepsilon_{max}$ : the allowed maximum margin will increase with the number of training epochs (see Appendix C), and the user only needs to monitor the training and validation accuracy curves. Although IMA is not perfect, it brings such a significant **benefit to the user: the ease of “adjusting”  $\varepsilon_{max}$  to make a trade-off between robustness and accuracy (simply set  $\beta=0.5$ ).**

From IMA, when an equilibrium state is reached, the distributions (i.e., local densities) of noisy samples in different classes are the same along the decision boundary (note: it does not necessarily mean the clean samples in different classes are equally spaced from the decision boundary). This is somewhat analog to Bayesian classification: at the optimal decision boundary, the distributions (densities) of samples in two classes are the same, assuming the classes have equal prior probabilities. From this perspective, the noisy samples, which are generated by IMA, serve as the surrogates of the real samples. Obviously, we cannot claim it is Bayesian classification because noisy samples may not reveal the true distributions. From this perspective, more advanced adversarial training methods may be developed such that the generated samples may reveal the true distributions (i.e.,  $p(x|y)$ ); if so, then the resulting decision boundary could be optimal and robust.

Additional Note: The validation accuracy curves of IMA in Fig. 8 in Appendix C increase and then gradually decrease. Please do not confuse this with the common concept of overfitting on clean data. Actually, when the models were trained with cross-entropy loss and clean data, there is no gradually-decreasing trend in validation accuracy curves, as shown in Fig. 11. Thus, the only explanation of the gradually-decreasing trend in Fig. 8 in Appendix C is margin overestimation.

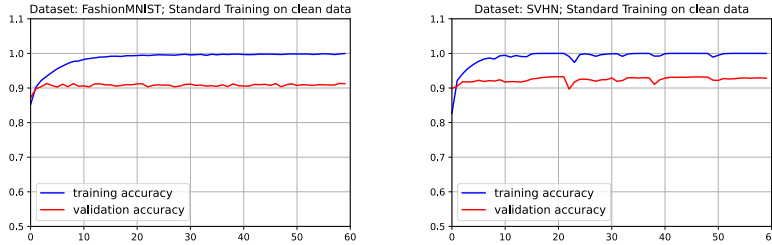


Figure 11: Training and validation accuracy curves (accuracy vs epoch) on the datasets, using standard training with cross-entropy loss and clean data. The accuracy scores are measured on clean data.

## E Further Discussion of the Equilibrium State

### E.1 The basic idea of our IMA method

If there are only two classes and the data samples are linearly separable, then linear SVM (support vector machine) will produce a linear decision boundary in the “middle” between the two classes. The decision boundary of SVM is robust against noises: the classification output will not change if a small amount of noise  $\delta$  is added to  $x$  as long as the vector norm of  $\delta$  is smaller than the margin of  $x$ . Here, the margin of  $x$  is the (minimum) distance between  $x$  and the decision boundary.

In general, the data samples in multiple classes are nonlinearly separable, and the robust decision boundary should be somewhere in the middle between classes, which is the goal that IMA pursues. The result on the Moons dataset shows that IMA can indeed produce a nonlinear decision boundary in the “middle” between classes. We use 2D Moons dataset because it is impossible to directly visualize a nonlinear decision boundary in a high dimensional space.

### E.2 The equilibrium state

Our IMA method is a heuristic-based method that is not derived from any theory. We use the equilibrium state analysis to provide a theoretical explanation of the method. We have shown that an equilibrium state can be achieved when the noisy samples have the same spatial distribution on the decision boundary. Here, we will analyze what will happen if the spatial distributions of the noisy samples in different classes are not the same on the current decision boundary. We note that our IMA method will actively generate and put noisy samples on (“close to” due to numerical precision) the current decision boundary of the neural network model, and the training is a dynamic process to adjust the decision boundary of

the model. Let's focus on the following two terms:

$$F_i \triangleq E_{X_n \in c_i \text{ and } X_n \in B_{ij}} = - \int q_i(x) \log(P_i(x)) dx \quad (9)$$

$$F_j \triangleq E_{X_n \in c_j \text{ and } X_n \in B_{ij}} = - \int q_j(x) \log(P_j(x)) dx \quad (10)$$

where  $q_i(x)$  and  $q_j(x)$  are the distributions (i.e., densities) of the noisy samples on the current decision boundary between the two classes, and  $q_i(x)$  and  $q_j(x)$  may not be equal to each other. In fact,  $F_i$  and  $F_j$  can be interpreted as two forces that try to expand the margins of the samples in the two classes against each other. By dividing the decision boundary into small regions (i.e., linear segments), the two integrals can be evaluated in the individual regions. In a region, if  $q_i(x) > q_j(x)$  (i.e., more samples in class-i) then the current state is not in equilibrium: after updating the model using these noisy samples, the noisy samples in class-i will be correctly classified and the noisy samples in class-j will be incorrectly-classified (this is a simple result of classification with imbalanced data in the region), which means the decision boundary will shift towards the samples in class-j, and therefore the margins of the corresponding samples in class-i will expand and the margins of the corresponding samples in class-j will shrink. Thus, the decision boundary may shift locally towards the samples in one of the classes. Obviously, the decision boundary will stop shifting when the local densities of noisy samples in different classes are the same along the decision boundary, i.e.,  $q_i(x)$  becomes equal to  $q_j(x)$ , which means an equilibrium state is reached.

## F Examples of Sample Images

### F.1 D2 Heart

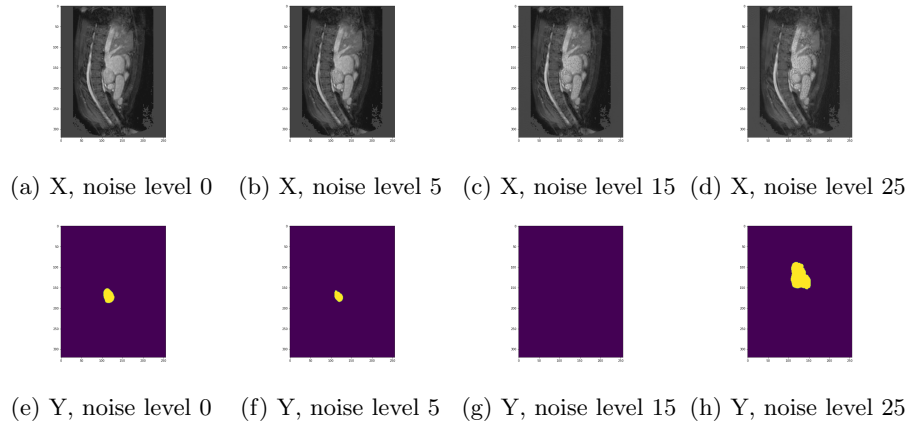


Figure 12: D2 Heart: The first row shows the input of nnUnet under different levels of 100-PGD adversarial noises. The second row shows the corresponding prediction of nnUnet under different levels of 100-PGD adversarial noises.

### F.2 D4 Hippocampus

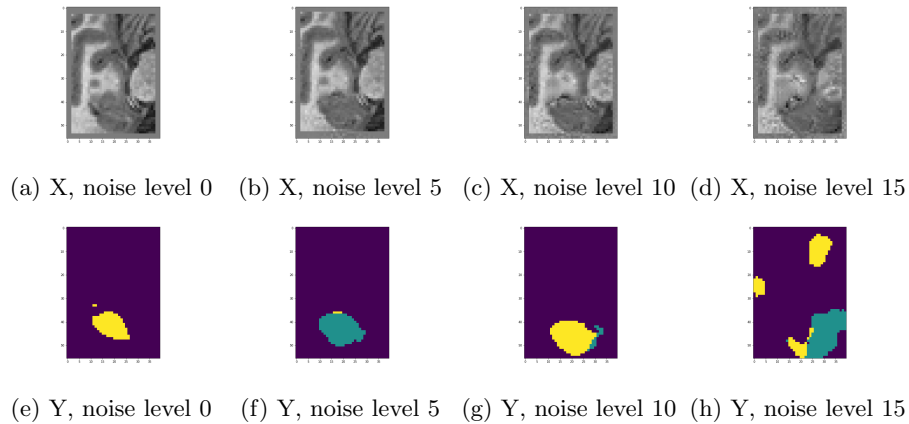


Figure 13: D4 Hippocampus: The first row shows the input of nnUnet under different levels of 100-PGD adversarial noises. The second row shows the corresponding prediction of nnUnet under different levels of 100-PGD adversarial noises.

### F.3 D5 Prostate

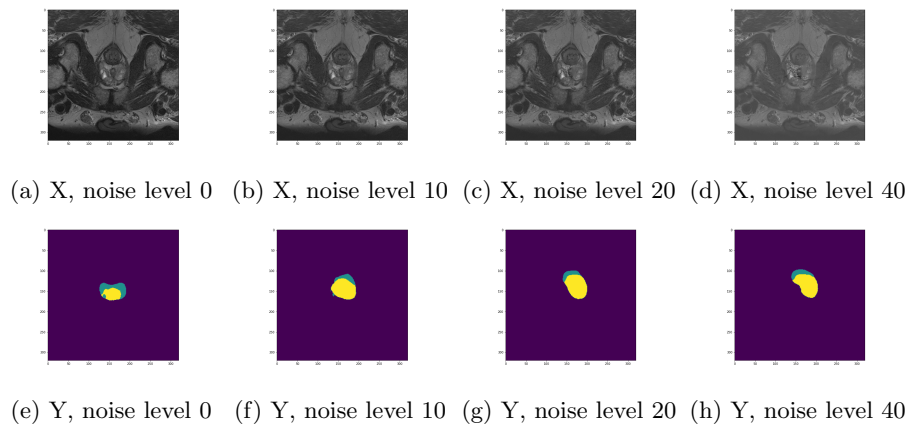


Figure 14: D5 Prostate: The first row shows the input of nnUnet under different levels of 100-PGD adversarial noises. The second row shows the corresponding prediction of nnUnet under different levels of 100-PGD adversarial noises.

## F.4 Covid-19 CT Images

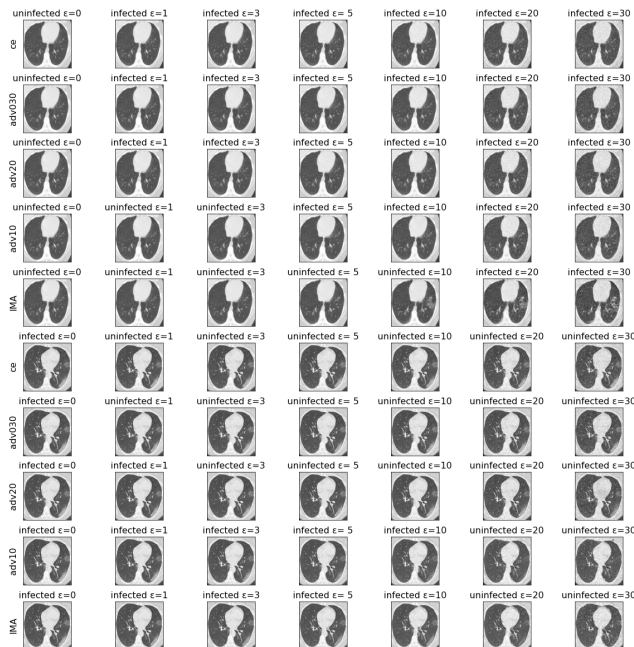


Figure 15: Each row shows a clean image and noisy images associated with a training method. The title of each image shows the predicted class label and the noise level. The clean images are correctly classified.

## G Details in experiments

### G.1 Classification Tasks

For the datasets of Moons, Fashion-MNIST, SVHN, CIFAR10 and COVID-19 CT,  $\beta$  in Algorithm 1 is 0.5 because robustness and accuracy are equally important [Goodfellow et al.(2015)Goodfellow, Shlens, and Szegedy]. In Algorithm 3,  $N_{PGD}$  is 20,  $N_{binary}$  is 10 and there is no repeat.  $\alpha$  in PGD is 4. Larger  $N_{PGD}$  and  $N_{binary}$  may lead to better convergence of the algorithms but more computing time. To make the comparison fair, the number of iterations and step size of TRADES are the same as those of the 20-PGD; and the number of PGD-iterations in MMA is 20. The number of iterations in DDN is 100, as suggested in [Rony et al.(2019)Rony, Hafemann, Oliveira, Ayed, Sabourin, and Granger]. Pytorch [Paszke et al.(2017)Paszke, Gross, Chintala, Chanan, Yang, DeVito, Lin, Desmaison, Antiga, and Lerer] is used for model implementation. Nvidia V100 and Titan V GPUs are used for model training and testing. All of the adversarial noises are measured in L2 norm.

In the Moons evaluation, for every method, we set the number of training



epochs to 30, maximum noise level to 0.3, and batch-size to 128; Adam optimizer was used with default parameters.

In the SVHN evaluation, training details are as follows. For all the methods, batch size was 128. For IMA, the number of training epochs was 60,  $\varepsilon_{max}$  was 2.0 and Adam optimizer was used with default parameters. For MMA and DDN, the number of training epochs was 60,  $\varepsilon_{max}$  was 2.0 and Adam optimizer was used with default parameters. For FAT, self-adjusted  $\tau$  was used as in [Zhang et al.(2020)Zhang, Xu, Han, Niu, Cui, Sugiyama, and Kankanhalli], the number of training epochs was 60 and SGD optimizer was used with parameters the same as those in [Zhang et al.(2020)Zhang, Xu, Han, Niu, Cui, Sugiyama, and Kankanhalli]. For GAIRAT, the number of training epochs was 60, “begin epoch” was 30 (half of the total number of epochs) and SGD optimizer was used with parameters the same as those in [Zhang et al.(2021)Zhang, Zhu, Niu, Han, Sugiyama, and Kankanhalli]. We set  $\varepsilon_{max}$  1.0 for FAT and 1.0 for GAIRAT, because FAT and GAIRAT with 2.0 cannot converge on this network. For TRADES, the number of training epochs was 60,  $\varepsilon_{max}$  was 2.0 and Adam optimizer was used with default parameters. Besides adversarial training, we did not use any other data augmentation (e.g. crop, etc.).

In the Fashion-FMNIST evaluation, training details are as follows. For all the methods, batch size was 128. For IMA, the number of training epochs was 60,  $\varepsilon_{max}$  was 5.0 and Adam optimizer was used with default parameters. For MMA and DDN, the number of training epochs was 60,  $\varepsilon_{max}$  was 5.0 and Adam optimizer was used with default parameters. For FAT,  $\varepsilon_{max}$  was 5.0, self-adjusted  $\tau$  was used as in [Zhang et al.(2020)Zhang, Xu, Han, Niu, Cui, Sugiyama, and Kankanhalli], the number of training epochs was 60 and SGD optimizer was used with parameters the same as those in [Zhang et al.(2020)Zhang, Xu, Han, Niu, Cui, Sugiyama, and Kankanhalli]. For GAIRAT,  $\varepsilon_{max}$  was 5.0, the number of training epochs was 60, “begin epoch” was 30 (half of the total number of epochs) and SGD optimizer was used with parameters the same as those in [Zhang et al.(2021)Zhang, Zhu, Niu, Han, Sugiyama, and Kankanhalli]. For TRADES, the number of training epochs was 60,  $\varepsilon_{max}$  was 5.0 and Adam optimizer was used with default parameters. Besides adversarial training, we did not use any other data augmentation (e.g. crop, etc.).

In the CIFAR10 evaluation, training details are as follows. The network was WideResNet-28-4 used in [Ding et al.(2020)Ding, Sharma, Lui, and Huang]. For all the methods, batch size was 128. For IMA,  $\varepsilon_{max}$  was 1.5 (in the main paper) and Adam optimizer was used with default parameters. Because of the complexity of this dataset, 100 training epochs were used for IMA, starting with a WideResNet-28-4 pre-trained on clean data. For MMA and DDN, we directly used the results from [Ding et al.(2020)Ding, Sharma, Lui, and Huang]. For FAT, self-adjusted  $\tau$  was used as in [Zhang et al.(2020)Zhang, Xu, Han, Niu, Cui, Sugiyama, and Kankanhalli], the number of training epochs was 100 and SGD optimizer was used with parameters the same as those in [Zhang et al.(2020)Zhang, Xu, Han, Niu, Cui, Sugiyama, and Kankanhalli]. For GAIRAT, the number of training epochs was 100, “begin epoch” was 50 (half of the total number of epochs) and SGD optimizer was used with parameters the same as

those in [Zhang et al.(2021)Zhang, Zhu, Niu, Han, Sugiyama, and Kankanhalli]. For TRADES, the number of training epochs was 100, and Adam optimizer was used with default parameters. The  $\varepsilon_{max}$  was 1.0 for MMA, DDN, FAT, GAIRAT and TRADES because  $\varepsilon_{max}$  of 1.5 led to a significant loss in the accuracy on clean data for these methods.

In the COVID-19 CT evaluation, training details are as follows. For all the methods, batch size was 32. For IMA, MMA, TRADES, DDN and “adv  $\varepsilon$ ”, the number of epochs is 40 and the maximum noise level for training ( $\varepsilon_{max}$ ) is 30. FAT and GAIRAT cannot converge in 40 epochs, so the two methods used 100 training epochs. The maximum noise level was 30 for IMA, MMA, DDN, TRADES, FAT and GAIRAT. Adam optimizer was used with default parameters. For “ce”, weight decay of 0.01 is applied with Adam (i.e., AdamW with default parameters).

## G.2 Segmentation Tasks

All of the models in the experiments are trained with 50 epochs, where each epoch is defined as 50 training iterations. The reason for selecting these three datasets, D2, D4 and D5, is that the sizes of these datasets are relatively small so that the models can stably converge within 50 training epochs. All of these three datasets are publically available. The experiments were conducted on Nvidia V100 GPUs. Other training details are the same as [Isensee et al.(2021)Isensee, Jaeger, Kohl, Petersen, and Maier-Hein].

# H Additional Supportive Results

## H.1 Robust Overfitting

The three tables, Table 26, Table 27 and Table 28 show that, for each evaluation, our proposed method IMA’s best checkpoint is always the last check point, which means that IMA does not have the robust overfitting problem [Rice et al.(2020)Rice, Wong, and Kolter, Kim et al.(2021)Kim, Lee, and Lee] in our experiment, due to the self-adaptive nature of IMA.

Table 26: IMA performance on SVHN validation set under 100-PGD attack with noise level=1.0

Epoch	9	19	29	39	49	59
noise=0	0.93	0.92	0.92	0.92	0.91	0.90
noise=1.0	0.13	0.22	0.27	0.29	0.31	0.33

Table 27: IMA performance on Fashion-MNIST validation set under 100-PGD attack with noise level=3.0

Epoch	9	19	29	39	49	59
noise=0	0.91	0.91	0.90	0.90	0.90	0.89
noise=3.0	0	0.08	0.20	0.27	0.31	0.33

Table 28: IMA performance on CIFAR10 validation set under 100-PGD attack with noise level=1.5

Epoch	9	19	29	39	49	59	69	79	89	99
noise=0	0.91	0.91	0.91	0.91	0.91	0.90	0.90	0.89	0.89	0.89
noise=1.5	0.0	0.0	0.05	0.09	0.13	0.17	0.17	0.20	0.21	0.21

## H.2 Black-box evaluation with SPSA

In this black-box evaluation, SPSA black-box adversarial attack [Uesato et al.(2018)Uesato, O’donoghue, Kohli, and Oord] was used. For all the methods, 2048 samples were generated for gradient estimation in SPSA. Because of the high time complexity of SPSA, only a subset from test set was used to evaluate. For SVHN and Fashion-MNIST, the first 10 samples from each class in the test set, a total of 100 samples, formed the new test set for SPSA. For CIFAR10, the first 100 samples, formed the new test set for SPSA. From Table 29, Table 30 and Table 31, IMA had a good resist to black-box adversarial attack, which means there was no gradient obfuscation in IMA [Uesato et al.(2018)Uesato, O’donoghue, Kohli, and Oord].

Table 29: Classification accuracy on SVHN (L2 norm in SPSA).

Noise	0.0	0.1	0.25	0.5	1.0
IMA	0.90	0.84	0.78	0.60	0.38
MMA	0.82	0.78	0.75	0.60	0.41

Table 30: Classification accuracy on F-MNIST (L2 norm in SPSA).

Noise	0.0	0.5	1.0	2.0	3.0
IMA	0.84	0.76	0.66	0.48	0.39
MMA	0.84	0.74	0.65	0.48	0.38

Table 31: Classification accuracy on CIFAR10 (L2 norm in SPSA).

Noise	0.0	0.5	1.0	1.5
IMA	0.93	0.64	0.41	0.24
MMA	0.87	0.64	0.4	0.22

## I TVDI and ADI

In the experiments, two metrics are used to evaluate the performance. The first one is “Total Voxel Dice Index (TVDI)”, which is given by:

$$TVDI = \frac{2 \times \sum_i^n TP_i}{2 \times \sum_i^n TP_i + \sum_i^n FP_i + \sum_i^n FN_i} \quad (11)$$

where the  $n$  is the number of samples in the testset,  $TP_i$  is the number of voxels in true positive area of the sample  $i$ ,  $FP_i$  is the number of voxels in false positive area of the sample  $i$  and  $FN_i$  is the number of voxels in false negative area of the sample  $i$ . The second metric is “Average Dice Index (ADI)”, whose formula is:

$$ADI = \sum_i^n \frac{2 \times TP_i}{2 \times TP_i + FP_i + FN_i} \times \frac{1}{n} \quad (12)$$

TVDI is the metric used in the original paper of nnUnet (Isensee et al. 2021). We used it to show that our results on clean data are similar to the reported results in (Isensee et al. 2021). However, in the TVDI metric, the individual samples do not have equal weights. We introduced ADI, a better metric to equally weight the samples, which also highlights the differences between the three methods. For simplicity, we use “clean TVDI/ADI” to refer to the metric score on clean data, and “noisy TVDI/ADI” to refer to the metric score on noisy data.